JAERI-M
88-115

LOWER HYBRID WAVE HEATING INTO NEUTRAL BEAM HEATED PLASMA IN THE JT-60 TOKAMAK

June 1988

Kenkichi USHIGUSA, Tsuyoshi IMAI, Yoshitaka IKEDA, Keiji SAKAMOTO
Franz X.SÖLDNER*, Yuichi TAKASE**, Shunji TSUJI, Katsuhiro SHIMIZU
Osamu NAITO, Kazuya UEHARA, Makoto AKIBA, Masanori ARAKI
Masayasu SATO, Hidetoshi YOSHIDA, Keisuke NAGASHIMA
Yoshinori KUSAMA, Hirotaka KUBO, Masahiro NEMOTO and Kenji TOBITA

日 本 原 子 力 研 究 所
Japan Atomic Energy Research Institute

JAERI-Mレポートは，日本原子力研究所が不定期に公刊している研究報告書です。
入手の問合わせは，日本原子力研究所技術情報部情報資料課（〒319-11茨城県那珂郡東海村）あて，お申しこしください。なお，このほかに財団法人原子力弘済会資料センター（〒319-11 茨城県那珂郡東海村日本原子力研究所内）で複写による実費頒布をおこなっております。

JAERI-M reports are issued irregularly.
Inquiries about availability of the reports should be addressed to Information Division Department of Technical Information, Japan Atomic Energy Research Institute, Tokai-mura, Naka-gun, Ibaraki-ken 319-11, Japan.

編集兼発行　日本原子力研究所
印　　刷　いばらき印刷㈱

JAERI-M 88-115

Lower Hybrid Wave Heating into Neutral Beam Heated Plasma in the JT-60 Tokamak

Kenkichi USHIGUSA, Tsuyoshi IMAI, Yoshitaka IKEDA[+]
Keiji SAKAMOTO[++], Franz X.SÖLDNER[*], Yuichi TAKASE[**]
Shunji TSUJI, Katsuhiro SHIMIZU, Osamu NAITO
Kazuya UEHARA[+], Makoto AKIBA[+], Masanori ARAKI[++]
Masayasu SATO, Hidetoshi YOSHIDA, Keisuke NAGASHIMA
Yoshinori KUSAMA, Hirotaka KUBO, Masahiro NEMOTO
and Kenji TOBITA

Department of Large Tokamak Research
Naka Fusion Research Establishment
Japan Atomic Energy Research Institute
Naka-machi, Naka-gun, Ibaraki-ken

(Received May 31, 1988)

Injection of high-power lower hybrid waves (LHW) of up to 6.0 MW into neutral-beam-20 MW-heated plasmas with the medium electron density regime ($\bar{n}_e \leq 3.5 \times 10^{19}$ m^{-3}) increases the plasma energy content at the same incremental energy confinement time as in the case of neutral beam heating alone. In addition to thermal electron and ion heating, LHW accelerates beam ions to energies considerably higher than the beam injection energy. In contrast to LH injection into OH plasmas in the same density regime, where substantial high-energy electron production is observed, the case of combined heating shows much less high-energy electrons. The heating efficiency of LHW in the combined heating case tends to decrease as the electron density is increased. Ray-tracing analysis suggests that the accessibility condition prevents effective heating in a high-density plasma. Estimation of wave damping, which is

---

+ Department of JT-60 Facility
++ Department of Thermonuclear Fusion Research
* Max-Planck-Institut für Plasmaphysic (FRG)
** Plasma Fusion Center, Massachusetts Institute of Technology (USA)

taking account of the beam component of the ion velocity distribution function, indicates that waves are absorbed by beam ions before they are absorbed by electrons.

Keywords: LHRF, NBI, JT-60, Wave-Particle Interaction, High Energy Ion Tail, High Energy Electron, Wave Damping Rate, Combined Heating

JT－60 トカマク中性子加熱プラズマへの低域混波成加熱

日本原子力研究所那珂研究所臨界プラズマ研究部

牛草　健吉・今井　剛・池田　佳隆[+]・坂本　慶司[++]・Franz X. SOLDNER[*]
高瀬　雄一[**]・辻　俊二・清水　勝宏・内藤　磨・上原　和也[+]
秋場　真人[+]・荒木　政則[++]・佐藤　正泰・吉田　英俊・永島　圭介
草間　義紀・久保　博孝・根本　正博・飛田　健次

（1988 年 5 月 31 日受理）

20 MWの中性粒子ビーム（NB）で加熱された，$\bar{n}_e < 3.5\times10^{19}\,m^{-3}$のプラズマに 6 MWまでの低域混成波を入射した結果，NB単独時と同じインクリメンタルエネルギー閉じ込め時間でプラズマの蓄積エネルギーが増加した。この時，電子温度，イオン温度の上昇とともに低域混成波が入射されたビームイオンを加速するのが観測された。同じ密度領域での低域混成波単独加熱時には，著しい高速電子の発生があるのに対し，複合加熱時には高速電子の発生が抑制される。複合加熱時の低域混成波の加熱効率は電子密度の上昇とともに減少するが，Ray軌跡解析の結果，この依存性は近接条件によるものと推定される。ビームイオンの寄与を考慮した波の減衰の評価の結果，複合加熱時には波が電子に吸収される前にビームイオンに吸収されることが示された。

那珂研究所：〒311－01 茨城県那珂郡那珂町大字向山 801－1
＋　JT－60 試験部
＋＋核融合研究部
＊　マックスプランクプラズマ物理研究所（FRG）
＊＊プラズマ核融合センターマサチューセッツ工科大学（USA）

Contents

目　　次

1. Introduction

Lower hybrid (LH) experiments in JT-60 have made new progress in steady-state current drive, profile control, and electron heating[1-4]. In particular, the combination of lower hybrid current drive (LHCD) and NB heating have shown a new possibility of improving the energy confinement time in NB-heated plasmas. Reduction in the internal inductance of the plasma by LHCD is correlated with the improvement and suppression of large m = 1 oscillations[3,4].

Simultaneous heating by LHW and NB is also interesting from the standpoint of interaction of LHW and beam ions. The acceleration of NB ions by the LHW has been observed in the ATC tokamak [5]. In the JIPPT-II tokamak, this interaction was confirmed, and the ion temperature increment in simultaneous heating agrees with the sum of those in the cases of individual heating [6]. Recent study of the interaction of LHW and beam ions in the ASDEX tokamak has shown that accelerated beam ions is enhanced when the wave perpendicular phase velocity is comparable to beam velocity [7]. The NB was tangentially injected in all these experiments. In the JT-60, 20 MW of neutral beams were injected almost perpendicularly, with a beam energy of around 75 keV. Although the bulk plasma parameters are in the electron heating regime for LHW with 2 GHz, the simultaneous injection of NB and LH causes a reduction in the wave-electron interaction and perpendicular acceleration of the beam ions. Theoretical estimation of wave damping in the combined heating, which is taking into account the beam tail on the ion velocity distribution function, predicts the change in wave-particle interaction in the combined heating consistently with experimental observations.

The experimental setup is described in Section 2. The experimental results are given in Section 3. Discussions and a summary are presented in Sections 4 and 5, respectively.

2. Experimental setup

Experiments on simultaneous heating by NB and LHW (NB + LH) in JT-60 (R_p = 3.1 m, a = 0.9 m [8,9]) were performed mainly with hydrogen plasma in the parameter ranges I_p = 1.5-2.4 MA, B_T = 4.0-4.8 T, and $\bar{n}_e$ = (2.0-6.0) × 10^{19} m^{-3}. TiC-coated molybdenum limiters and divertor

1. Introduction

Lower hybrid (LH) experiments in JT-60 have made new progress in steady-state current drive, profile control, and electron heating[1-4]. In particular, the combination of lower hybrid current drive (LHCD) and NB heating have shown a new possibility of improving the energy confinement time in NB-heated plasmas. Reduction in the internal inductance of the plasma by LHCD is correlated with the improvement and suppression of large m = 1 oscillations[3,4].

Simultaneous heating by LHW and NB is also interesting from the standpoint of interaction of LHW and beam ions. The acceleration of NB ions by the LHW has been observed in the ATC tokamak [5]. In the JIPPT-II tokamak, this interaction was confirmed, and the ion temperature increment in simultaneous heating agrees with the sum of those in the cases of individual heating [6]. Recent study of the interaction of LHW and beam ions in the ASDEX tokamak has shown that accelerated beam ions is enhanced when the wave perpendicular phase velocity is comparable to beam velocity [7]. The NB was tangentially injected in all these experiments. In the JT-60, 20 MW of neutral beams were injected almost perpendicularly, with a beam energy of around 75 keV. Although the bulk plasma parameters are in the electron heating regime for LHW with 2 GHz, the simultaneous injection of NB and LH causes a reduction in the wave-electron interaction and perpendicular acceleration of the beam ions. Theoretical estimation of wave damping in the combined heating, which is taking into account the beam tail on the ion velocity distribution function, predicts the change in wave-particle interaction in the combined heating consistently with experimental observations.

The experimental setup is described in Section 2. The experimental results are given in Section 3. Discussions and a summary are presented in Sections 4 and 5, respectively.

2. Experimental setup

Experiments on simultaneous heating by NB and LHW (NB + LH) in JT-60 (R_p = 3.1 m, a = 0.9 m [8,9]) were performed mainly with hydrogen plasma in the parameter ranges I_p = 1.5-2.4 MA, B_T = 4.0-4.8 T, and $\bar{n}_e$ = (2.0-6.0) × 10^{19} m^{-3}. TiC-coated molybdenum limiters and divertor

plates were replaced by graphite ones at the last shutdown. During these experiments the vacuum vessel was kept at wall temperatures of 200-300 °C. Apart from several limiter shots for reference purpose, almost all experiments were carried out in divertor discharges since they allow better density control. The hydrogen NB, with power of up to 20 MW at a beam energy of 75 keV, was injected with injection angles of 74° and 108° to the magnetic axis before application of the LH power.

JT-60 has three LH units [10]. The total generator power is 24 MW with a pulse length of up to 10 s. Up to now the maximum time-averaged torus input power of around 9.5 MW (the peak value being 11 MW) has been injected into the plasma, and a power of about 2 MW with an RF pulse duration of 8 s has been successfully injected. Two units (units A and B) are optimized for the heating experiments, and the other (unit C) is optimized for the current drive. Each unit has an antenna consisting of an array of 8 waveguides toroidally and 4 waveguides poloidally. The width w, the height h, and the spacing s of the waveguides are shown in Table 1. Figure 1 shows the launched $N_{||}$ spectra calculated by the Brambilla code [11] for each unit shown in Table 1. Unit C excites mainly waves of $N_{||}$ = 1.0-2.5 at the toroidal phasing of $\Delta\phi = 90°$, and units A and B yield $N_{||}$ = 1.4-2.4 at $\Delta\phi = 180°$. Launchers are located in the scrape-off plasma, typically 1-2 cm outside the separatrix surface. Coupling characteristics of the launchers show qualitative agreement with the Brambilla theory, and the reflection coefficient for each unit is less than 20 % in normal divertor discharges. All experiments reported in this paper were performed at a wave frequency of 2 GHz.

3. Experimental Results

A typical example of the combined heating in a 2 MA divertor plasma is shown in Fig. 2. An NB power of 18 MW with a beam energy of 75 keV is injected into a divertor plasma with $\overline{n_e} \cong 1.5 \times 10^{19}$ m^{-3}. RF power of 4.7 MW, which is launched from unit A (2.3 MW, $\Delta\phi = 180°$) and unit B (2.4 MW, $\Delta\phi = 180°$), is applied 0.5 s after the onset of NB pulse. The diamagnetic measurement shows that 4.7 MW of LH power increases the plasma energy content to 1.95 MJ from 1.65 MJ ($\Delta W \cong 0.3$ MJ). The electron density increases to $\overline{n_e} = 3.5 \times 10^{19}$ m^{-3} from $\overline{n_e} = 2.5 \times 10^{19}$ m^{-3} during the LH pulse. This density rise reduces the shine-through power

plates were replaced by graphite ones at the last shutdown. During these experiments the vacuum vessel was kept at wall temperatures of 200-300 °C. Apart from several limiter shots for reference purpose, almost all experiments were carried out in divertor discharges since they allow better density control. The hydrogen NB, with power of up to 20 MW at a beam energy of 75 keV, was injected with injection angles of 74° and 108° to the magnetic axis before application of the LH power.

JT-60 has three LH units [10]. The total generator power is 24 MW with a pulse length of up to 10 s. Up to now the maximum time-averaged torus input power of around 9.5 MW (the peak value being 11 MW) has been injected into the plasma, and a power of about 2 MW with an RF pulse duration of 8 s has been successfully injected. Two units (units A and B) are optimized for the heating experiments, and the other (unit C) is optimized for the current drive. Each unit has an antenna consisting of an array of 8 waveguides toroidally and 4 waveguides poloidally. The width w, the height h, and the spacing s of the waveguides are shown in Table 1. Figure 1 shows the launched $N_{||}$ spectra calculated by the Brambilla code [11] for each unit shown in Table 1. Unit C excites mainly waves of $N_{||}$ = 1.0-2.5 at the toroidal phasing of $\Delta\phi = 90°$, and units A and B yield $N_{||}$ = 1.4-2.4 at $\Delta\phi = 180°$. Launchers are located in the scrape-off plasma, typically 1-2 cm outside the separatrix surface. Coupling characteristics of the launchers show qualitative agreement with the Brambilla theory, and the reflection coefficient for each unit is less than 20 % in normal divertor discharges. All experiments reported in this paper were performed at a wave frequency of 2 GHz.

3. Experimental Results

A typical example of the combined heating in a 2 MA divertor plasma is shown in Fig. 2. An NB power of 18 MW with a beam energy of 75 keV is injected into a divertor plasma with $\overline{n_e} \cong 1.5 \times 10^{19}$ m^{-3}. RF power of 4.7 MW, which is launched from unit A (2.3 MW, $\Delta\phi = 180°$) and unit B (2.4 MW, $\Delta\phi = 180°$), is applied 0.5 s after the onset of NB pulse. The diamagnetic measurement shows that 4.7 MW of LH power increases the plasma energy content to 1.95 MJ from 1.65 MJ ($\Delta W \cong 0.3$ MJ). The electron density increases to $\overline{n_e} = 3.5 \times 10^{19}$ m^{-3} from $\overline{n_e} = 2.5 \times 10^{19}$ m^{-3} during the LH pulse. This density rise reduces the shine-through power

and increases the absorbed NB power by 0.9 MW. The corresponding increase in the stored energy $\Delta W'_{NB}$ can be estimated as $\Delta W'_{NB} = \tau_E^{INC}|_{NB} \cdot \Delta P_{NB}$, where $\tau_E^{INC}|_{NB}$ is the incremental energy confinement time for the NB in the combined heating. It is confirmed experimentally that the value of $\tau_E^{INC}|_{NB}$ in the combined heating is almost the same as that for NB heating alone ($\tau_E^{INC}|_{NB} \cong 54$ ms). In this case one gets $\Delta W'_{NB} \cong 0.05$ MJ. The heating efficiency for the LH, $\Delta W_{LH}/P_{LH} \equiv (\Delta W - \Delta W'_{NB}) / P_{LH}$, is around 53 ms, this being almost the same as $\tau_E^{INC}|_{NB}$. The charge exchange neutral analyzer located on the outside of torus shows that high energy ion fluxes I_{CX} of up to $\sim$ 160 keV is formed by LH. The ion temperature measured from the Doppler broadening of the TiXXI line, T_i^{XXI}, increases by 2 keV, and the ion temperature deduced from forward scattering of the 190 keV helium beam, T_i^{AB} agrees with T_i^{XXI}. The hard X-ray emission from the plasma center with energies higher than 260 keV increases during initial 100 ms of the LH pulse and immediately decreases afterwards. The intensity of the hard X-ray emission in this case is lower than that for LH heating of OH plasmas under almost the same conditions. The electron cyclotron emission (ECE) shows almost thermal spectra during most of the LH pulse duration. Although the time evolution of the second harmonic ECE, $I_{2\omega ce}$, indicates that there is no appreciable increase in the electron temperature, the stored energy of the thermal electrons increases in accordance with the density increment. These observations show that the heating mechanism for combined heating is quite different from that for LH heating of OH plasmas.

In Fig. 3, the total energy content of the plasma is plotted as a function of total input power where open symbols are for NB only and closed symbols are for NB+LH. All data plotted in Fig. 3 were obtained in divertor discharges with $\overline{n_e} < 4.0 \times 10^{19}$ m^{-3}. The total energy content was measured with the diamagnetic loop. Within a scatter of 10 %, they agree with results obtained with the confinement analysis code based on kinetic measurement (LOOK/OFMC/SCOOP [12]). In the total input power, the NB power P_{NB}^{abs} is the absorbed power where shine-through and re-ionization losses has been subtracted, while the LH power P_{LH}^{IN} is the torus input power. As shown in Fig. 3, up to 6 MW of LH power increases the plasma energy content linearly with almost the same incremental energy confinement time as with NB heating. The gross energy confinement time of NB+LH heated plasma shows a typical L-mode degradation with respect to the total input power in the same way as NB heating

[8,9]. Several shots with NB+LH heating show H-mode phenomena [9,13], namely the decrease in H_α emission from the main and the divertor chamber, the increase in electron density with a flattening of the profile, the increase in plasma energy content, the decrease in high-frequency magnetic fluctuations near the X-point. The improvement of energy confinement is less than 10 % in the H-mode phase. Since description of these H-mode phenomena is beyond the scope of this paper, only L-mode data are plotted in Fig. 3.

The heating efficiency of LHW in combined heating depends on the electron density. Figure 4 shows the density dependence of the heating efficiency $\Delta W_{LH} / \Delta P_{LH}$, where the above-mentioned correction for the change in NB shine-through power has been performed. The heating efficiency $\Delta W_{LH} / \Delta P_{LH}$ at $\overline{n_e} \leq 3.5 \times 10^{19}$ m^{-3} is about 50 ms, which is comparable to NB heating ($\tau_E^{INC}|_{NB} \cong 54$ msec), while $\Delta W_{LH} / \Delta P_{LH}$ is less than 20 ms at higher densities ($\overline{n_e} > 5.0 \times 10^{19}$ m^{-3}). The heating efficiency of the LHW decreases with increasing electron density and NB+LH heating is effective only at $\overline{n_e} < 3.5 \times 10^{19}$ m^{-3}. As we discuss later in Section 4, the density dependence of the heating efficiency is consistent with the accessibility condition for the LHW.

The electron temperature near the plasma center (r/a $\sim$ 0.1), measured by Thomson scattering, is plotted as a function of ($P_{OH} + P_{NB}^{abs} + P_{LH}^{IN}$) / $\overline{n_e}$ in Fig. 5. The electron temperatures in the combined heating case are higher than those in NB heating alone by $\sim$1 keV. There is no large difference in the electron heating rate between NB heating and the combined heating. The electron heating rate is roughly $\eta_{EH} \equiv \overline{n_e}\, T_{eo} / (P_{OH} + P_{NB}^{abs} + P_{LH}^{IN}) \sim 0.5 \pm 0.2 \times 10^{19}$ m^{-3} keV/MW in both cases, while $\eta_{EH} \sim$ (2-3) $\times 10^{19}$ m^{-3} keV/MW for LHEH without NB [4]. A similar plot for the ion temperature T_i^{AB} measured by forward scattering of helium beam is shown in Fig. 6. The ion heating rate, $\eta_{IH} \equiv \overline{n_e}\, T_{io} / (P_{OH} + P_{NB}^{abs} + P_{LH}^{IN})$, is around 0.8×10^{19} m^{-3} keV/MW.

Figure 7 shows the stored thermal electron energy W_e and the stored ion thermal energy W_i versus the total stored energy W^{KIN}, where triangles and circles represent NB heating and the combined heating, respectively. W_e is determined from the electron temperature profile measured with a six-point Thomson scattering system and the electron density profile measured with four-channel interferometers. W_i is estimated from the transport analysis with the assumption that the ion thermal conductivity $\chi_i = C_i \cdot \chi_i^{NC}$, where C_i is the 'neo-classical

multiplier' and χ_i^{NC} is the neoclassical ion thermal conductivity [14]. C_i is determined from the central ion temperature measured by helium active-beam scattering and C_i becomes typically 10-15 in the case of combined heating. Z_{eff} which is estimated from the visible bremsstrahlung radiation, is used for the analysis. There is no large difference on Z_{eff} between NB alone and LH+NH ($Z_{eff} \cong 3.0$-4.0 at $\overline{n_e} = (2.0$-$3.5) \times 10^{19}$ m^{-3}). The power deposition profile due to the neutral beam is calculated by the Orbit Following Monte Carlo (OFMC) code [15], and we have assumed that the RF power is absorbed only by electrons. OFMC estimates that the beam component of the plasma energy content to be around 40 % in this density range ($2.1 < \overline{n_e}$ (10^{19} m^{-3}) < 2.5) . The electron thermal stored energy in the combined heating is around 35 % of the total energy content. The energy partition ratios W_e / W^{KIN} and W_i / W^{KIN} in combined heating are almost the same as those of NB heating alone under similar conditions. In Fig. 8 the total energy content estimated by the above mentioned procedure (W^{KIN}) is compared with the diamagnetically determined energy content (W^*). W^{KIN} is systematically smaller than W^* by 10-20 %. This discrepancy is considered to be significant because W^{KIN} agrees with W^* by within 10 % in the case of NB heating alone. In estimating W^{KIN}, it was assumed that the LH power is absorbed only by electrons. The enhancement of the high-energy ion tail is observed experimentally, which may increase the beam component of the total stored energy. Furthermore, the collisional relaxation of the enhanced ion tail on thermal ions is not taken into account in the confinement analysis code. The systematic difference between W^{KIN} and W^* suggests that the enhanced beam energy and a modification of ion power deposition profile caused by LH injection may contribute to the increase in the stored energy in combined heating.

Acceleration of beam ion by LH is observed with two charge exchange neutral particle analyzers. Figure 9 shows the arrangement of charge exchange analyzers. One of the analyzers (CX-A system) is located on the outer side (divertor side) of the torus and view the plasma at a tangential radius of $r/a \sim 0.3$ almost perpendicularly ($\sim 85°$) to the magnetic field at a poloidal angle of $\sim 30°$ with respect to the midplane. The charge exchange process in this viewing chord is dominated in the peripheral region near the outer limiters, where strong refuelling of neutral particles from the divertor chamber is observed by H_α measurements [16]. The other analyzer (CX-B system) vertically views the

plasma center from the top of torus. The viewing chord of the CX-B analyzer is located at the same toroidal section as NB lines (NBI units #9 and #10). It has been shown that this analyzer observes neutrals which are charge-exchanged mainly with halo-neutrals near the plasma center [17], because the observation field of the analyzer crosses a beam heating zone near the center.

Figure 10 (a) and (b) show charge exchange spectra for the same shot as shown in Fig. 2 measured with the CX-A and CX-B analyzers, respectively. Neutral fluxes at NB heating phase are denoted as open circles, while closed circles show fluxes at NB+LH heating phase. The enhancem nt of beam ion tail is observed in both analyzers and this suggests that LH accelerates beam ions not only in the peripheral region of plasm but also in the central region. Accelerated ions have a tail temperature of $\sim$ 15 keV and the acceleration of beam ions of up to $\sim$ 160 keV is observed in the CX-A analyzer.

The density dependence of the plasma hard X-ray radiation (E > 260 keV) along the central chord normalized by the LH power I_{HX} / P_{LH} is shown in Fig. 11 for the case of LHEH of OH plasma (closed symbols) and for the case of combined heating (open symbols). In the previous series of experiments carried out during Jan.-Mar. 1987, TiC-coated Mo limiters and divertor plates were employed. They were all replaced with graphite ones prior to the last series of experiments carried out during Jun.-Oct. 1987. The hard X-ray radiation for the discharges with graphite walls is larger than that with TiC-coated Mo walls and this is considered to be due to the higher Z_{eff}. The value of I_{HX} / P_{LH} for LH alone in hydrogen discharges with graphite walls is close to that in helium discharges with TiC-coated Mo walls. It can be seen that the hard X-ray radiation is reduced in the combined heating case in comparison to the case of LHEH alone. The reduction in hard X-ray signal in the combined heating tends to become larger at higher electron density.

The reduction in wave-electron interaction is also confirmed by the ECE measurements. The time evolutions of electron temperatures at $r/a \sim 0$, 0.3 and 0.6 measured by ECE are shown in Fig. 12(a). The ECE signal is considerably affected by high-energy electrons and usually does not show a thermal spectrum in low density LHEH experiments. We cannot regard the intensity of the second harmonic ECE as proportional to the electron temperature in such cases. Figure 12(b) shows the ECE spectrum at $t \sim 5.39$ s when LH and NB are injected simultaneously.

Typical non-thermal spectrum observed in a low density LHEH experiment is also plotted as a broken line for reference. The observed spectrum does not have the distinctive features of a superthermal spectrum, i.e., there is no large down shift of harmonics and the intensity is not enhanced over the thermal spectrum. The time evolution of ECE spectrum is shown in Fig. 12(c). The enhanced emission at $f \sim 1.5\ f_{ceo}$ is observed during the first 0.1 s of the LH pulse. With the exception of this weakly non-thermal emission, the ECE spectrum is not affected by high energy electrons. The intensity of ECE at 1.5 times the central electron cyclotron frequency normalized by the LH power, $I_{ECE}(1.5f_{ceo}) / P_{LH}$, is plotted as a function of the electron density in Fig. 13, where closed and open symbols represent the LH alone and the combined heating cases, respectively. Since $I_{ECE}(1.5f_{ceo})$ is sensitive to high energy electron population, Fig. 13 shows that simultaneous injection of NB reduces high energy electrons caused by LH consistently with measurements of hard X-ray radiation.

4. Discussions

Experimental observations in the combined heating strongly suggest that the reduction in interaction of LH waves with electrons relates to the enhancement of the beam tail by LH. A possibility of the change in wave-particl interaction is discussed theoretically in this section.

Beam heated plasmas in JT-60 have a perpendicular beam ion tail because neutral beams are injected almost perpendicularly. A LH wave with $N_{||} \fallingdotseq 2.4$, which is the maximum $N_{||}$ of launched LH waves by units A and B, has the perpendicular refractive index $N_{\perp}$ of around 79 at $n_e = 4 \times 10^{19}\ m^{-3}$ and $B_T = 4.8$ T. This $N_{\perp}$ corresponds to a hydrogen energy of about 75 keV. Therefore it can be easily expected that launched LH waves interact with beam ions. In order to show a possibility of the change in wave-particle interaction in the combined heating, a wave damping rate due to beam ions should be compared with that due to bulk electrons.

For the estimation of the wave damping rate in the combined heating, we assume an electrostatic approximation and unmagnetized ions. Furthermore we neglect a contribution of beam ions to the real part of the dispersion relation because we assume that the beam ion density n_B

Typical non-thermal spectrum observed in a low density LHEH experiment is also plotted as a broken line for reference. The observed spectrum does not have the distinctive features of a superthermal spectrum, i.e., there is no large down shift of harmonics and the intensity is not enhanced over the thermal spectrum. The time evolution of ECE spectrum is shown in Fig. 12(c). The enhanced emission at $f \sim 1.5\ f_{ceo}$ is observed during the first 0.1 s of the LH pulse. With the exception of this weakly non-thermal emission, the ECE spectrum is not affected by high energy electrons. The intensity of ECE at 1.5 times the central electron cyclotron frequency normalized by the LH power, $I_{ECE}(1.5f_{ceo}) / P_{LH}$, is plotted as a function of the electron density in Fig. 13, where closed and open symbols represent the LH alone and the combined heating cases, respectively. Since $I_{ECE}(1.5f_{ceo})$ is sensitive to high energy electron population, Fig. 13 shows that simultaneous injection of NB reduces high energy electrons caused by LH consistently with measurements of hard X-ray radiation.

4. Discussions

Experimental observations in the combined heating strongly suggest that the reduction in interaction of LH waves with electrons relates to the enhancement of the beam tail by LH. A possibility of the change in wave-particl interaction is discussed theoretically in this section.

Beam heated plasmas in JT-60 have a perpendicular beam ion tail because neutral beams are injected almost perpendicularly. A LH wave with $N_{||} \doteqdot 2.4$, which is the maximum $N_{||}$ of launched LH waves by units A and B, has the perpendicular refractive index $N_{\perp}$ of around 79 at $n_e = 4 \times 10^{19}\ m^{-3}$ and $B_T = 4.8$ T. This $N_{\perp}$ corresponds to a hydrogen energy of about 75 keV. Therefore it can be easily expected that launched LH waves interact with beam ions. In order to show a possibility of the change in wave-particle interaction in the combined heating, a wave damping rate due to beam ions should be compared with that due to bulk electrons.

For the estimation of the wave damping rate in the combined heating, we assume an electrostatic approximation and unmagnetized ions. Furthermore we neglect a contribution of beam ions to the real part of the dispersion relation because we assume that the beam ion density n_B

is much less than the bulk ion density n_i. The dispersion relation under these assumptions is given by [18]

$$D_{ES} = S\frac{k_\perp^2}{k^2} + P\frac{k_{||}^2}{k^2} - \frac{3}{2}\frac{\omega_{pi}^2}{\omega^4}k^2v_{Ti}^2 - \frac{3}{8}\frac{\omega_{pe}^2}{\omega_{ce}^4}k^2v_{Te}^2 \tag{1}$$

$$+ i\left[\frac{k_{||}^2}{k^2}\frac{\omega_{pe}^2}{\omega^2}F\left(\frac{\omega}{k_{||}v_{Te}}\right) + \frac{\omega_{pi}^2}{\omega^2}F\left(\frac{\omega}{kv_{Ti}}\right) + \pi\frac{\omega_{pB}^2}{k^2}\left.\frac{\partial f_B}{\partial v}\right|_{v=\frac{\omega}{k}}\right]$$

where $S = 1 + (\omega_{pe}/\omega_{ce})^2 - (\omega_{pi}/\omega)^2$, $P = 1 + (\omega_{pe}/\omega)^2 - (\omega_{pi}/\omega)^2$ and $F(x) = 2(\pi)^{1/2}x^3\exp(-x^2)$. $\omega_{pe}/2\pi$, $\omega_{pi}/2\pi$, $\omega_{ce}/2\pi$ and $\omega/2\pi$ are the electron and ion plasma frequencies, the electron cyclotron frequency and the wave frequency, respectively. $v_{Te} = (2T_e/m_e)^{1/2}$, $v_{Ti} = (2T_i/m_i)^{1/2}$, $k_\perp$ and $k_{||}$ are the electron and ion thermal velocities, the perpendicular wave number and the parallel wave number. $\omega_{pB} = (e^2n_B/\varepsilon_0m_H)^{1/2}$ is the beam ion plasma angular frequency (proton). f_B is the velocity distribution function of beam ions.

We model the beam distribution function by

$$f_B = \begin{cases} f_{B0} & ; \ |v| \leq v_B \\ f_{B0}\exp\{-(v^2 - v_B^2)/v_{TB}^2\} & ; \ |v| \geq v_B \end{cases} \tag{2}$$

where $v_{TB} = (2T_B/m_H)^{1/2}$, $v_B = (2E_B/m_H)^{1/2}$. E_B and T_B are the injected beam energy and the beam tail temperature. f_{B0} is calculated from

$$\int_{-\infty}^{+\infty} f_B dv = 1 \ .$$

The damping rate is calculated in the weak damping limit to be

$$\gamma_e = \frac{2\sqrt{\pi}}{\frac{\partial D_{ES}}{\partial\omega}}\frac{k_{||}^2}{k^2}\frac{\omega_{pe}^2}{\omega^2}\left(\frac{\omega}{k_{||}v_{Te}}\right)^3\exp\left[-\left(\frac{\omega}{k_{||}v_{Te}}\right)^2\right]$$

$$\gamma_i = \frac{2\sqrt{\pi}}{\frac{\partial D_{ES}}{\partial\omega}}\frac{\omega_{pi}^2}{\omega^2}\left(\frac{\omega}{kv_{Ti}}\right)^3\exp\left[-\left(\frac{\omega}{kv_{Ti}}\right)^2\right] \tag{3}$$

$$\gamma_B = \frac{2\sqrt{\pi}C_0}{\frac{\partial D_{ES}}{\partial \omega}} \frac{\omega_{pB}^2}{\omega^2} \left(\frac{\omega}{kv_{TB}}\right)^3 \exp\left[-\left(\frac{\omega}{kv_{TB}}\right)^2 + \left(\frac{v_B}{v_{TB}}\right)^2\right]$$

where

$$C_0^{-1} = \frac{2}{\sqrt{\pi}} \frac{v_B}{v_{TB}} + \exp\left(\frac{v_B^2}{v_{TB}^2}\right) \mathrm{Erfc}\left(\frac{v_B}{v_{TB}}\right) ,$$

$$\mathrm{Erfc}(x) = \frac{2}{\sqrt{\pi}} \int_x^\infty e^{-\xi^2} d\xi$$

The beam ion density n_B can be estimated by using results of the OFMC code. The beam stored energy is described by

$$W_B = 2\pi R_p \int_0^a 2\pi r\, dr\, n_B(0)\left(1 - \frac{r^2}{a^2}\right)^{\alpha_B} \int_0^\infty 2\pi v_\perp \frac{1}{2} m_H v_\perp^2 dv_\perp \qquad (4)$$

where R_p and a are the major and minor radii. The profile factor α_B of beam ions and W_B are calculated by the OFMC code. From Eqs(4) and (2), the central beam ion density $n_B(0)$ can be described by

$$n_B(0) = \frac{(\alpha_B + 1)W_B}{\pi R_p \pi a^2 E_B} \frac{1 + \frac{T_B}{E_B}}{1 + 2\left(\frac{T_B^2}{E_B^2}\right)\left(1 + \frac{E_B}{T_B}\right)} \qquad (5)$$

In typical LH＋NB heated plasma, $W_B \sim 0.4$ MJ, $\alpha_B \sim 0.3$, $E_B = 75$ keV, $R_p = 3.1$ m, a = 0.9 m and $n_e(0) \sim 4 \times 10^{19}$ m^{-3} and the beam tail temperature measured by the charge exchange neutral analyzer shows $T_B \sim 15$ keV. Then $n_B(0) \sim 1.4 \times 10^{18}$ m^{-3} and $n_B(0)/n_e(0) \sim 0.035$ are obtained in this estimation.

Figure 14 shows the damping rates due to beam ions (γ_B), bulk electrons (γ_e) and bulk ions (γ_i) as a function of $N_{||}$, where $n_e = 4 \times 10^{19}$ m^{-3}, $B_T = 4.8$ T, $T_e = 5$ keV, $T_i = 7$ keV, $T_B = 15$ keV, $E_B = 75$ keV, $W_B = 0.4$ MJ and $\omega/2\pi = 2$ GHz. In this model, γ_B becomes zero at $N_{||} \sim 2.4$ because $\partial f_B/\partial v = 0$ at $\omega/k = v_B$. The damping rate γ_B is larger than γ_e at all $N_{||}$ regime of $N_{||} < 2.4$. The ratio γ_B/γ_e is around 10^3 at

$N_{||} \sim 1.7$, which is about the mean of $N_{||}$ launched from units A, B ($\Delta\phi$ = 180°) and unit C ($\Delta\phi$ = 90°) as shown in Fig. 1. Therefore it can be expected that the wave damping due to beam ions is dominant from the combined heating parameters. At $N_{||} = 2.0$, the central beam density of $n_B(0) \sim 1.8 \times 10^{17}$ m^{-3} leads to $\gamma_B \sim \gamma_e$ from this parameters and this beam density corresponds to $n_B(0)/n_e(0) \sim 0.005$.

The density dependence of damping rates is shown in Fig. 15, where $N_{||} = 2.0$ and other parameters are the same as Fig. 14. At low density regime ($n_e < 2.5 \times 10^{19}$ m^{-3}), the electron damping rate γ_e becomes larger than γ_B. This indicates that the electron damping becomes dominant at low density regime even in the combined heating. As shown in Fig. 11 and Fig. 13, the hard X-ray radiation and ECE signal show that the reduction of high energy electrons occurs only at $\overline{n_e} > (1.5 - 2.0) \times 10^{19}$ m^{-3} and at lower density regime the electron damping can be expected with the same way as LHEH alone. Therefore Fig. 15 is qualitatively consistent with measurements of the hard X-ray radiation and ECE.

Results of a ray-tracing code, which includes the damping effect due to beam ions, are shown in Fig. 16 for $N_{||0} = 2.2$ in typical parameters of the combined heating. Although the damping rate is calculated under the assumption of electrostatic approximation, the warm electromagnetic dispersion relation is used to solve the ray trajectory. Solid and broken lines show results with and without NB heating. In the case without NB, the dominant part of the damping rate γ is γ_e, while $\gamma \sim \gamma B$ in the case with NB. The deposition region in the case with NB shifts outward because of its large damping rate. Without NB, waves which have smaller $N_{||}$ does not damp fully through single-path propagation because $\omega/k_{||} >> v_{Te}$. However almost all wave component with exception of non-accessible waves can be absorbed by beam ions in the case with NB. A typical wave deposition profile to beam ions, P_{iB}, is shown in Fig. 17, where launched spectra of units A and B are calculated by the Brambilla code for $\Delta\phi$ = 180° and the input power of RF is 6 MW. About 4 MW of RF power is absorbed by beam ions through single-path propagation and this corresponds to ∿65% of input power. The non-accessible power is around 1.5 MW in this case. The deposition profile $p_{iB}(r)$ is localized near the half radius. It should be noted that significant part of RF input power can be absorbed by plasma through single-path propagation without the up-shift of $N_{||}$ following multiple reflections

from the plasma surface[19].

Figure 18 shows $I_{ECE}(1.5\omega_{ce})/P_{LH}$ as a function of the electron density for various beam energies. It can be found that $I_{ECE}(1.5\omega_{ce})/P_{LH}$ does not depend strongly on the injected beam energy. This does not contradict with the above mentioned modelling. From Eq.(3) we can obtain the critical electrol density n_{ec} for the transition from electron to beam ion absorption ($\gamma_e = \gamma_i$). In Fig. 19, n_{ec} is plotted as a function of the beam energy E_B for the same parameters as in Fig. 15. Since n_{ec} has very weak dependence on the beam energy, it may not be found large difference on observed ECE signals as the beam energy is changed.

We discuss the density dependence of the heating efficiency for LH in the combined heating. As shown in Fig. 4, the heating efficiency for LH in the combined heating decreases as the electron density is increased. LHEH experiments of OH plasmas in JT-60 have shown that the heating efficiency correlates with the accessibility condition at half radius [4], and the detected maximum energy of the hard X-ray radiation coincides with the critical energy determined from the accessibility condition at half radius [2]. The fraction of accessible power within the half radius $\eta_{acc} \equiv P_{acc}/P_{in}$ in the case of combined heating is plotted as a function of electron density in Fig. 20. The heating efficiency shown in Fig. 4 is also plotted for comparison. The accessible power for the excited wave spectra under the same parameters as Fig. 17 is calculated using the ray tracing code. Solid and broken lines show the accessible power fractions for waves excited by two units (A and B) and by three units (A, B and C), respectively. The heating efficiency of LH in the combined heating has very similar dependence on electron density as the accessible power fraction as half radius. Although it may be possible to explain the density dependence of heating efficiency by other mechanisms, the accessibility seems to be a very probable explanation.

Finally we comment on the problem of applying LHCD in NB heated plasmas. Stabilization of sawtooth by LHCD has been reported from many machines [20-23], and provides an attractive way of achieving high temperatures and good confinement in the central region of plasma. It has been demonstrated in JT-60 [1,3,4] and ASDEX [23] that the combination of LHCD and NB heating improves energy confinement of beam heated plasmas. In such applications one has to be select plasma parameters

so that the LH wave does not couple to the beam ions. For example in JT-60, $\overline{n_e} \leq 1.5 \times 10^{19}$ m^{-3} is required to drive RF current efficiency in the NB heated hydrogen plasmas.

5. Conclusions

The NB + LH combined heating experiments in JT-60 can be concluded in the following way.

(1) The LH power increases the plasma energy content at the same incremental energy confinement time as with NB heating alone in the density regime $\overline{n_e} \leq 3.5 \times 10^{19}$ m^{-3}.

(2) Increases in the central electron and ion temperatures are observed ($\Delta T_e(0) \leq 1$ keV, $\Delta T_i(0) \leq 2$ keV) with $P_{LH} \leq 6$ MW, $\overline{n_e} \sim 3.0 \times 10^{19}$ m^{-3}.

(3) The energy partition of the kinetically estimated stored energy for the combined heating case is almost the same as that for NB heating alone at the same density regime. The discrepancy between the kinetically estimated energy and the magnetically measured energy suggests that the enhanced beam energy and a modification of ion power deposition profile caused by LH injection may increase 10-20 % of the total energy.

(4) The interaction of the LH wave with electron is reduced in the combined heating case compared to the case of LHEH alone, and a significant enhancement of the ion tail beyond the beam injection energy is observed.

(5) The heating efficiency by LH in combined heating decreases at higher densities and LH is effective only in the density regime $\overline{n_e} \leq 3.5 \times 10^{19}$ m^{-3}.

(6) The estimation of wave damping rates in combined heating shows waves are absorbed by beam ions before they are absorbed by electrons. The density dependence of the heating efficiency of LH is consistent with the accessibility condition at half radius.

so that the LH wave does not couple to the beam ions. For example in JT-60, $\overline{n_e} \leq 1.5 \times 10^{19}$ m^{-3} is required to drive RF current efficiency in the NB heated hydrogen plasmas.

5. Conclusions

The NB＋LH combined heating experiments in JT-60 can be concluded in the following way.

(1) The LH power increases the plasma energy content at the same incremental energy confinement time as with NB heating alone in the density regime $\overline{n_e} \leq 3.5 \times 10^{19}$ m^{-3}.

(2) Increases in the central electron and ion temperatures are observed ($\Delta T_e(0) \leq 1$ keV, $\Delta T_i(0) \leq 2$ keV) with $P_{LH} \leq 6$ MW, $\overline{n_e} \sim 3.0 \times 10^{19}$ m^{-3}.

(3) The energy partition of the kinetically estimated stored energy for the combined heating case is almost the same as that for NB heating alone at the same density regime. The discrepancy between the kinetically estimated energy and the magnetically measured energy suggests that the enhanced beam energy and a modification of ion power deposition profile caused by LH injection may increase 10-20 % of the total energy.

(4) The interaction of the LH wave with electron is reduced in the combined heating case compared to the case of LHEH alone, and a significant enhancement of the ion tail beyond the beam injection energy is observed.

(5) The heating efficiency by LH in combined heating decreases at higher densities and LH is effective only in the density regime $\overline{n_e} \leq 3.5 \times 10^{19}$ m^{-3}.

(6) The estimation of wave damping rates in combined heating shows waves are absorbed by beam ions before they are absorbed by electrons. The density dependence of the heating efficiency of LH is consistent with the accessibility condition at half radius.

Acknowledgements

The authors would like to acknowledge Drs. Y. Shimomura, M. Nagami, and M. Azumi for fruitful discussions. They would like to thank all members of the JT-60 team for their contribution, and Drs. S. Mori, K. Tomabechi, M. Yoshikawa and S. Tamura for continued encouragement and support.

References

[1] IMAI, T. and JT-60 TEAM, in Plasma Physics and Controlled Nuclear Fusion Research 1986 (Proc. 11th Int. Conf. Kyoto, 1986), Vol. 1, IAEA, Vienna (1987) 563, IMAI, T., USHIGUSA, K., SAKAMOTO, K., IKEDA, Y., FUJII, T. et al., Current Drive And Confinement Studies Of LHRF Experiments On JT-60, to be published in Nucl. Fusion (1988).

[2] SAKAMOTO, K. and JT-60 TEAM, in Controlled Fusion and Plasma Physics (Proc. 14th Eur. Conf. Madrid, 1987), Vol. 11D, Part III, Madrid (1987) 894.

[3] TSUJI, S. and JT-60 TEAM, in Controlled Fusion and Plasma Physics (Proc. 14th Eur. Conf. Madrid, 1987), Vol. 11D, Part I, Madrid (1987) 57.

[4] YOSHINO, R. and JT-60 TEAM, Plasma Phys. and Control. Fusion 29 (1987) 1377.

[5] KRITZ, A.H., MAHAJAN, S.M., BERGER, R.L., GOLDSTONE, R.J., MOTLEY, R.W., HOOK, W.M., BERNABEI, S., Nucl. Fusion 18 (1978) 835.

[6] NODA, N., KANEKO, O., OHKUBO, K., SUGIHARA, R., KAWAHATA, K., SAKURAI, K., OKA, Y., KAWASUMI, K., TANAHASHI, S., FUJITA, J., Experiment On Heating With Simultaneous Injection Of Neutral-Beam And Lower Hybrid Waves In The JIPPT-II Torus, Rep. of Institute of Plasma Physics, Nagoya Univ., IPPJ-567 (1982).

[7] RYTER, F., BROCKEN, H., IZVOZCHIKOV, A., LEUTERER, F., MAASSBERG, H., MAYER, H.M., et al., in Controlled Fusion and Plasma Physics (Proc. 13th Eur. Conf. Schliersee, 1986), Vol. 10C, Part I, Schliersee (1986) 101.

[8] NAGAMI, M. and JT-60 TEAM, in Plasma Physics and Controlled Nuclear Fusion Research 1986 (Proc. 11th Int. Conf. Kyoto, 1986), Vol. 1, IAEA, Vienna (1987) 89.

Acknowledgements

The authors would like to acknowledge Drs. Y. Shimomura, M. Nagami, and M. Azumi for fruitful discussions. They would like to thank all members of the JT-60 team for their contribution, and Drs. S. Mori, K. Tomabechi, M. Yoshikawa and S. Tamura for continued encouragement and support.

References

[1] IMAI, T. and JT-60 TEAM, in Plasma Physics and Controlled Nuclear Fusion Research 1986 (Proc. 11th Int. Conf. Kyoto, 1986), Vol. 1, IAEA, Vienna (1987) 563, IMAI, T., USHIGUSA, K., SAKAMOTO, K., IKEDA, Y., FUJII, T. et al., Current Drive And Confinement Studies Of LHRF Experiments On JT-60, to be published in Nucl. Fusion (1988).

[2] SAKAMOTO, K. and JT-60 TEAM, in Controlled Fusion and Plasma Physics (Proc. 14th Eur. Conf. Madrid, 1987), Vol. 11D, Part III, Madrid (1987) 894.

[3] TSUJI, S. and JT-60 TEAM, in Controlled Fusion and Plasma Physics (Proc. 14th Eur. Conf. Madrid, 1987), Vol. 11D, Part I, Madrid (1987) 57.

[4] YOSHINO, R. and JT-60 TEAM, Plasma Phys. and Control. Fusion 29 (1987) 1377.

[5] KRITZ, A.H., MAHAJAN, S.M., BERGER, R.L., GOLDSTONE, R.J., MOTLEY, R.W., HOOK, W.M., BERNABEI, S., Nucl. Fusion 18 (1978) 835.

[6] NODA, N., KANEKO, O., OHKUBO, K., SUGIHARA, R., KAWAHATA, K., SAKURAI, K., OKA, Y., KAWASUMI, K., TANAHASHI, S., FUJITA, J., Experiment On Heating With Simultaneous Injection Of Neutral-Beam And Lower Hybrid Waves In The JIPPT-II Torus, Rep. of Institute of Plasma Physics, Nagoya Univ., IPPJ-567 (1982).

[7] RYTER, F., BROCKEN, H., IZVOZCHIKOV, A., LEUTERER, F., MAASSBERG, H., MAYER, H.M., et al., in Controlled Fusion and Plasma Physics (Proc. 13th Eur. Conf. Schliersee, 1986), Vol. 10C, Part I, Schliersee (1986) 101.

[8] NAGAMI, M. and JT-60 TEAM, in Plasma Physics and Controlled Nuclear Fusion Research 1986 (Proc. 11th Int. Conf. Kyoto, 1986), Vol. 1, IAEA, Vienna (1987) 89.

[9] NAGAMI, M. and JT-60 TEAM, Recent Results From JT-60, Research Rep. of Japan Atomic Energy Research Institute, JAERI-M87-205 (1987).

[10] NAGASHIMA, T., UEHARA, K., KIMURA, H., IMAI, T., FUJII, T., et al., Fusion Eng. Design 5 (1987) 101.

[11] BRAMBILLA, M., Nucl. Fusion 16 (1976) 47.

[12] KIKUCHI, M., HIRAYAMA, T., SIMIZU, K., TANI, K., YOSHIDA, H., et al., Nucl. Fusion 27 (1987) 1239.

[13] NAKAMURA, H., TSUJI, S., et al., H-mode Studies in JT-60 Outside X-point Divertor, to be submitted to Nucl. Fusion.

[14] CHANG, C.S., HINTON, F.L., Phys. Fluids 25 (1982) 1493.

[15] TANI, K., AZUMI, M., OHTSUKA, M., KISHIMOTO, H., TAMURA, S., in Heating in Toroidal Plasmas (Proc. Joint Varenna-Grenoble Int. Symp. Grenoble 1978), Vol. 1 (1978) 31.

[16] YAMADA, K., TSUJI, S., SHIMIZU, K., NISHITANI, T., NAGASHIMA, K. and JT-60 TEAM, Nucl. Fusion 27 (1987) 1203.

[17] KIMURA, H. and JT-60 TEAM, in Controlled Fusion and Plasma Physics (Proc. 14th Eur. Conf. Madrid, 1987), Vol. 11D, Part III, Madrid (1987) 857.

[18] STIX, T.H., Theory of Plasma Waves, McGraw-Hill, New York, 1962.

[19] BONOLI, P.T., PORKOLAB, M., TAKASE, Y., KNOWLTON, S.F., Numerical Modelling of Lower Hybrid RF Heating and Current Drive Experiments in the Alcator C Tokamak, MIT Plasma Fusion Center Report PFC/JA-83-37, accepted for publication in Nucl. Fusion (1988).

[20] CHU, T.-K., BELL, R., BERNSBEI, S., CAVALLO, A., GUHARAY, S., et al., Nucl. Fusion 26 (1986) 666.

[21] KNOWLTON, S., PORKOLAB, M., TAKASE, Y., Nucl. Fusion 28 (1988) 99.

[22] VAN HOUTTE, D., BRIFFOD, G., CHABERT, P., GORMEZANO, C., HOW, T., et al., Nucl. Fusion 24 (1984) 1485.

[23] SÖLDNER, F.X., MCCORMIC, K., ECKHARTT, D., KORNHERR, M., LEUTERER, et al., Phys. Rev. Lett. 57 (1986) 1137.

Table 1 Antenna Parameters

Unit		A	B	C
Purpose		Heating	Heating	CD
Poloidal location angle	(deg)	-40	40	40
Width of single w.g.	(cm)	2.0	2.0	1.6
Height of single w.g.	(cm)	11.5	11.5	11.5
Width of wall	(cm)	1.0	1.0	0.6
Typical phasing $\Delta\phi$	(deg)	180	180	90
Mean $N_{\parallel}$ at typical phasing		1.9	1.9	1.7
Spectrum width $\Delta N_{\parallel}$		1.0	1.0	1.5
Achieved power density	(kW/cm^2)	3.1	2.8	6.8
Achieved Total power	(MW)	3.3	3.0	4.0

All units: 4 rows of 8 waveguides each.

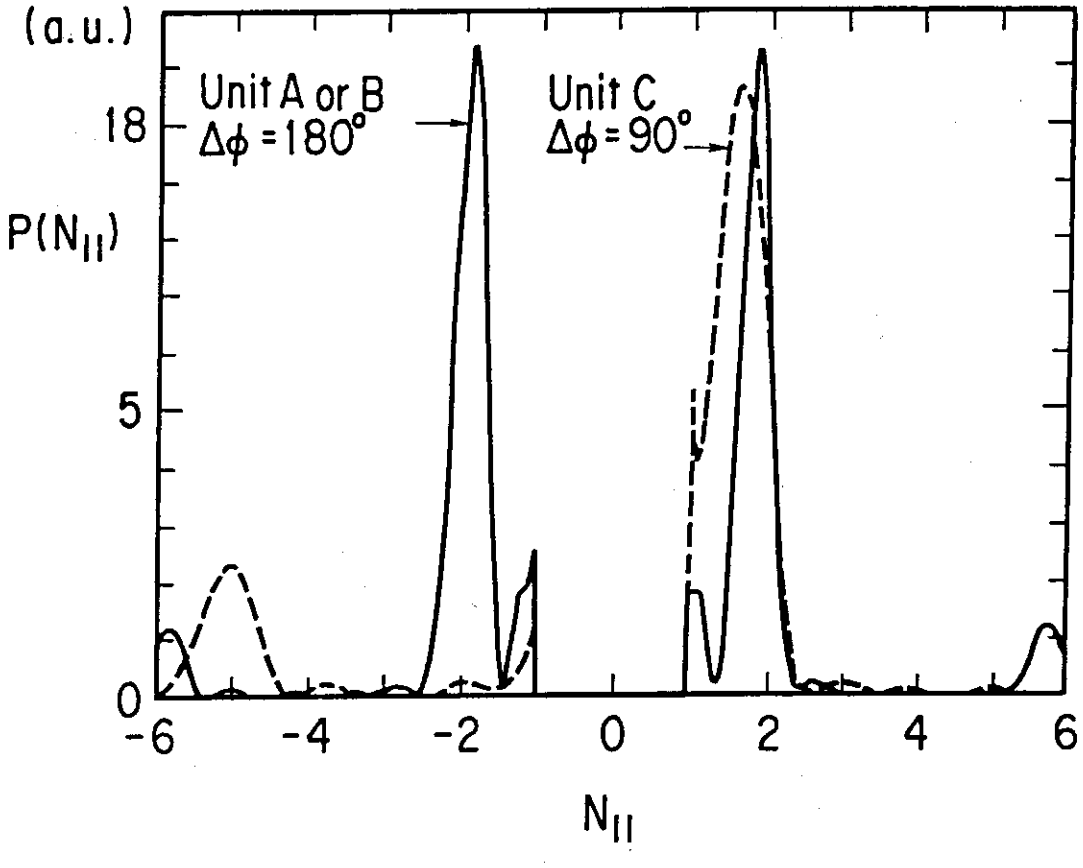

Fig. 1 Excited wave spectra for units A and B at $\Delta\phi$ = 180°, and for unit C at $\Delta\phi$ = 90°.

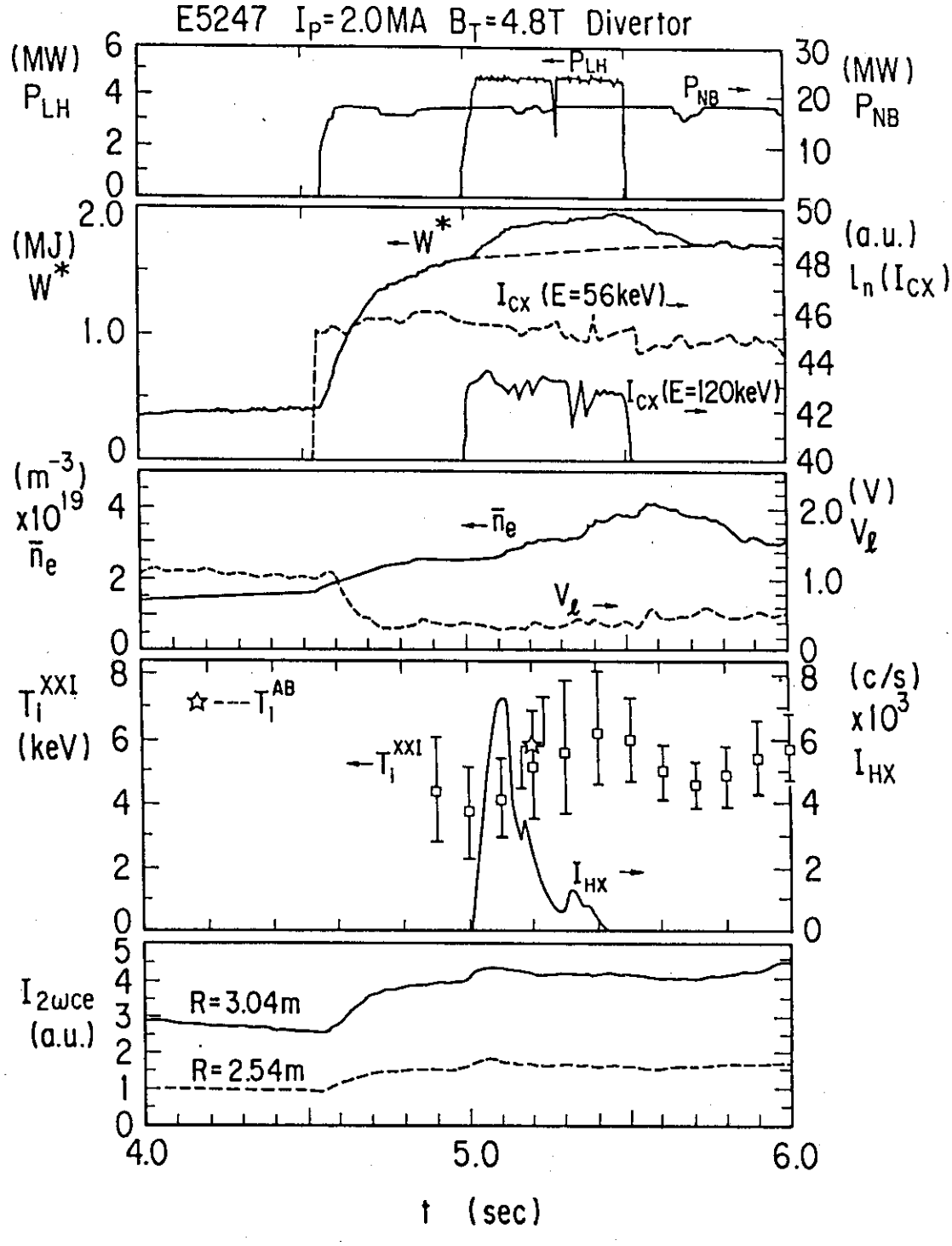

Fig. 2 A typical example of LH+NB combined heating. W^*, I_{cx}, T_i^{XXI}, T_i^{AB}, I_{HX} and $I_{2\omega ce}$ represent the plasma energy content, the charge exchange flux, the ion temperature measured by Doppler broadening of Ti^{XXI} line, the ion temperature measured by forward scattering of He beam, the hard X-ray radiation (E > 260 keV), and the second harmonic ECE emission, respectively.

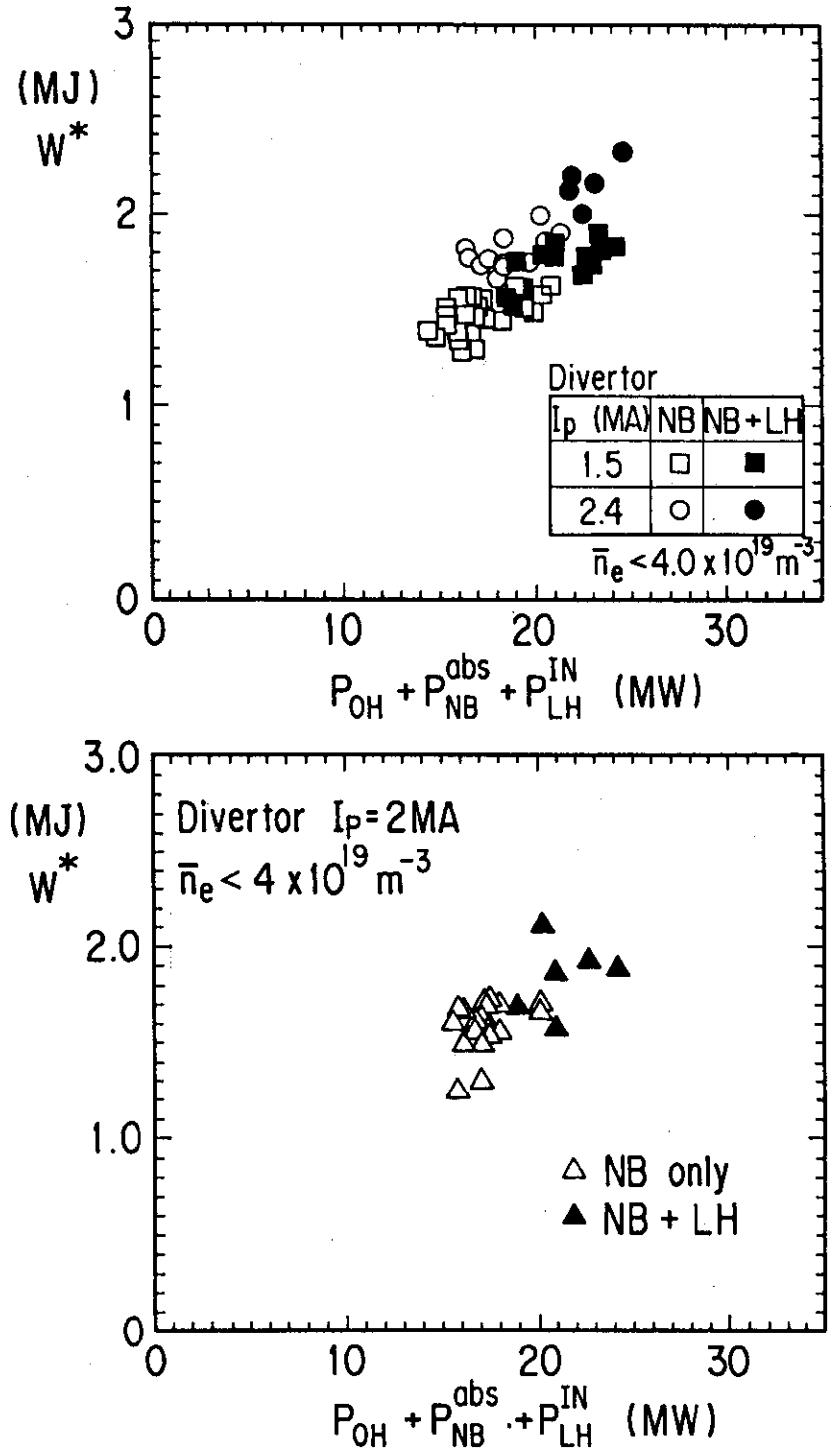

Fig. 3 Plasma energy content W^* against the total heating power $P_{OH} + P_{NB}^{abs} + P_{LH}^{IN}$ where P_{NB}^{abs} is the absorbed NB power and P_{LH}^{IN} is the torus input power of LH. (a); I_p = 1.5, 2.4 MA, (b); I_p = 2.0MA.

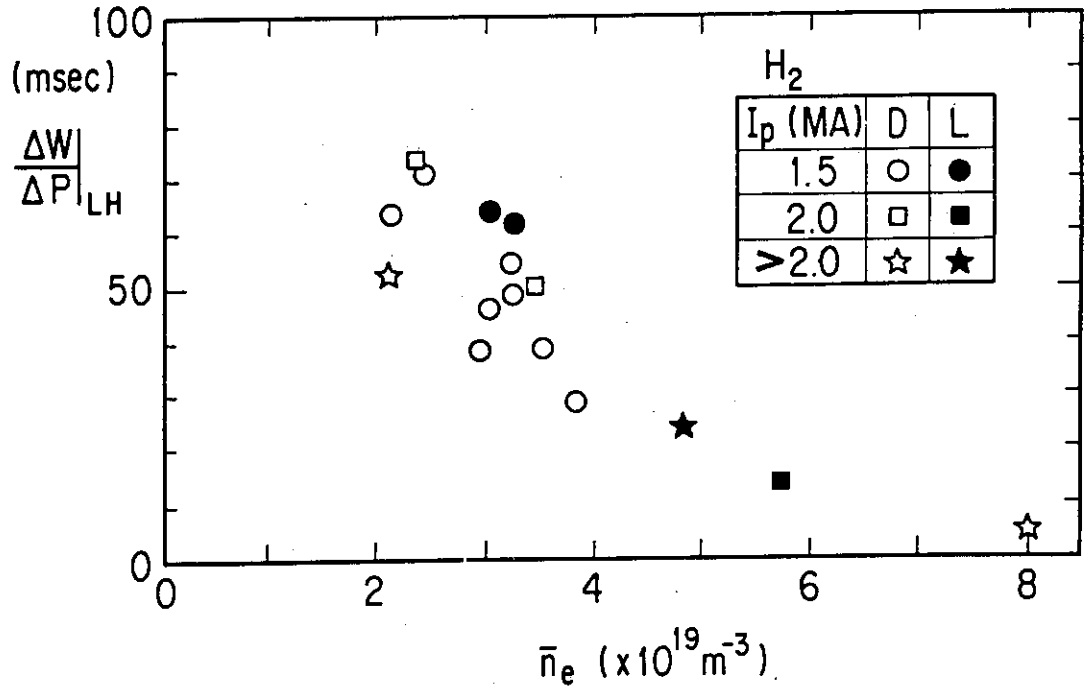

Fig. 4 Heating efficiency of LH, $\Delta W/\Delta P|_{LH}$, against electron density $\overline{n_e}$.

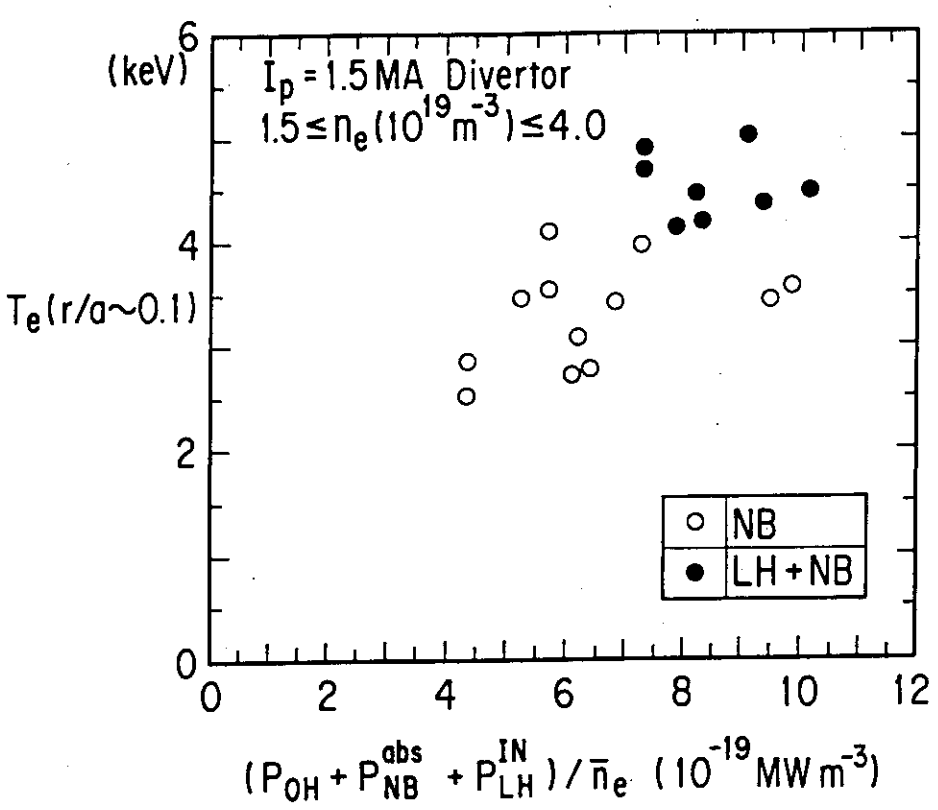

Fig. 5 The electron temperature near the plasma center ($r/a \sim 0.1$) measured by Thomson scattering as a function of $(P_{OH} + P_{NB}^{abs} + P_{LH}^{IN})/\overline{n_e}$.

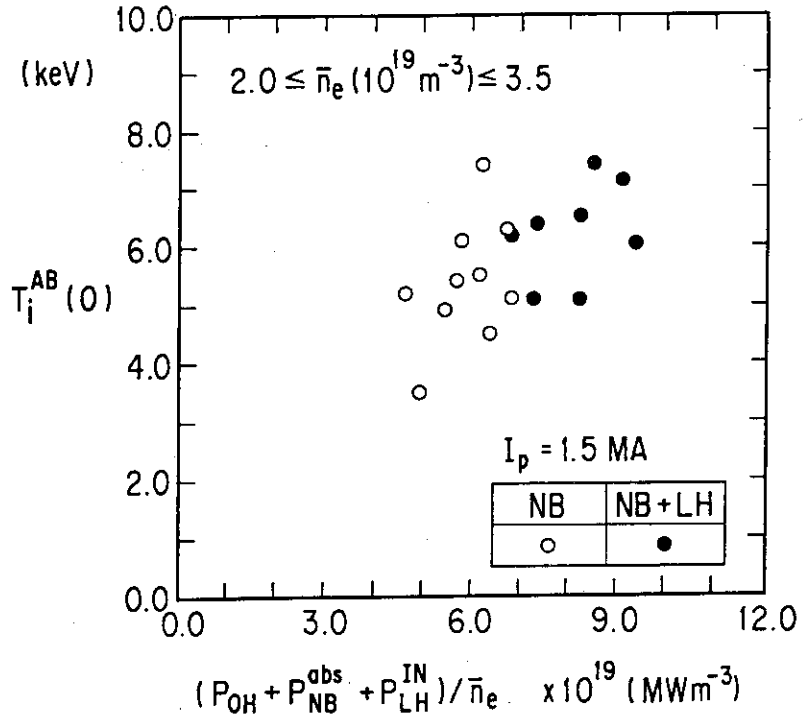

Fig. 6 The central ion temperature measured by active beam scattering against $(P_{OH} + P_{NB}^{abs} + P_{LH}^{IN})/\overline{n_e}$

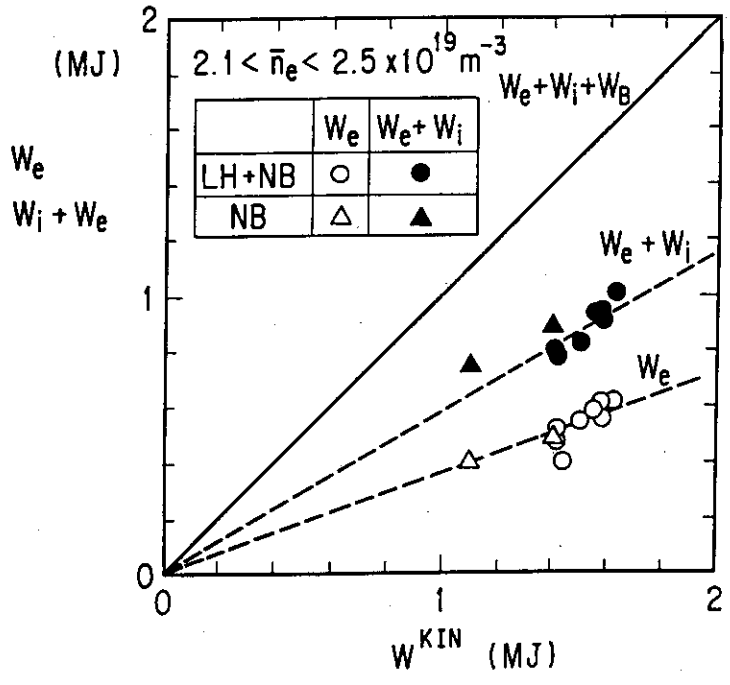

Fig. 7 The energy partition of the kinetically estimated stored energy. W_e, W_i and W^{KIN} are the thermal electron stored energy, the thermal ion stored energy and the total stored energy, respectively. P_{LH} = 2.5 - 5.7 MW, P_{NB}^{abs} = 13 - 15 MW for LH+NB.

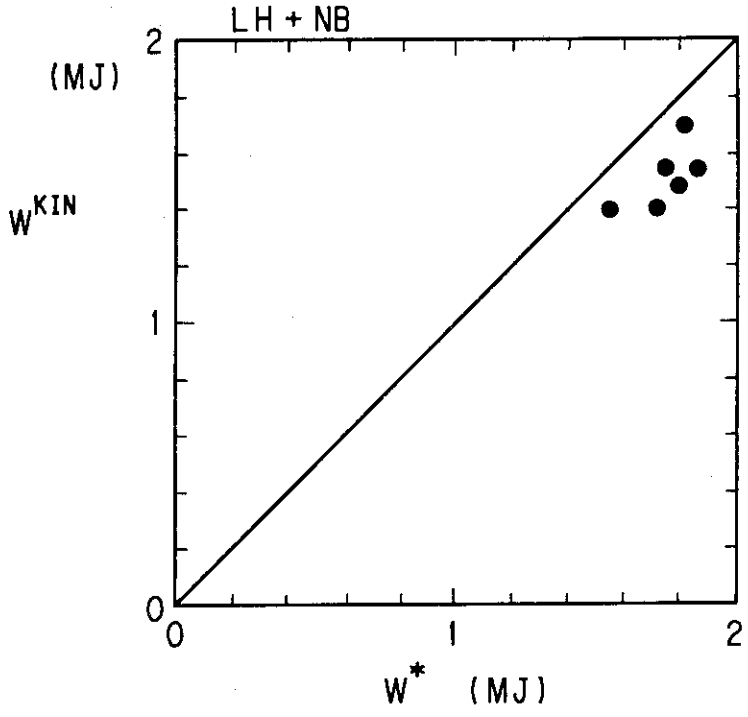

Fig. 8 The kinetically estimated stored Energy W^{KIN} versus magnetically measured sotred energy W^*.

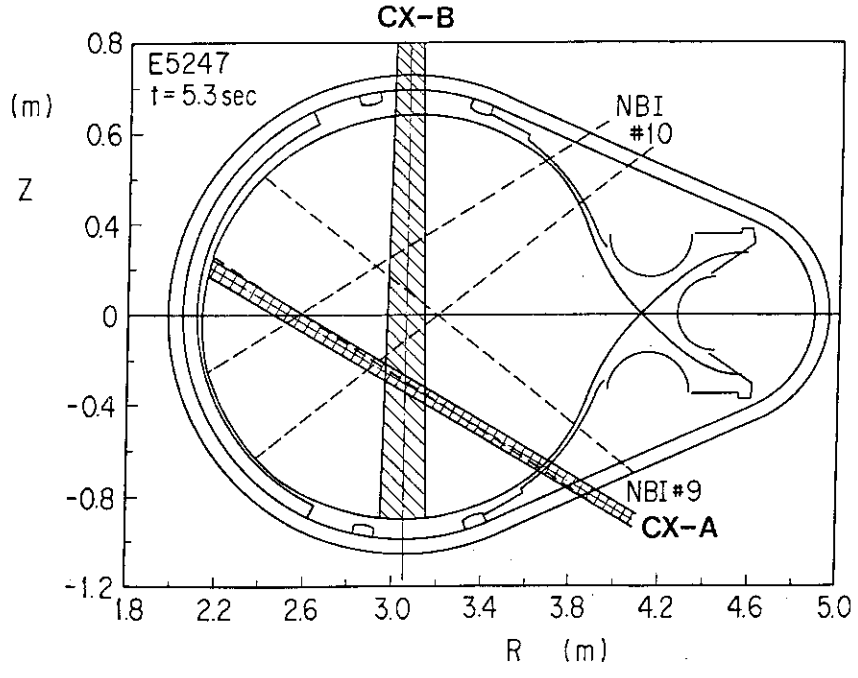

Fig. 9 The arrangement of charge exchange measurements. The charge exchange process in this viewing chord of CX-A analyzer is dominated in the peripheral region near the outer limiters. The viewing chord of CX-B analyzer locates at the same toroidal section as NB lines (NBI units #9 and #10) and this analyzer observes neutrals which are charge-exchanged mainly with halo-neutrals near the plasma center.

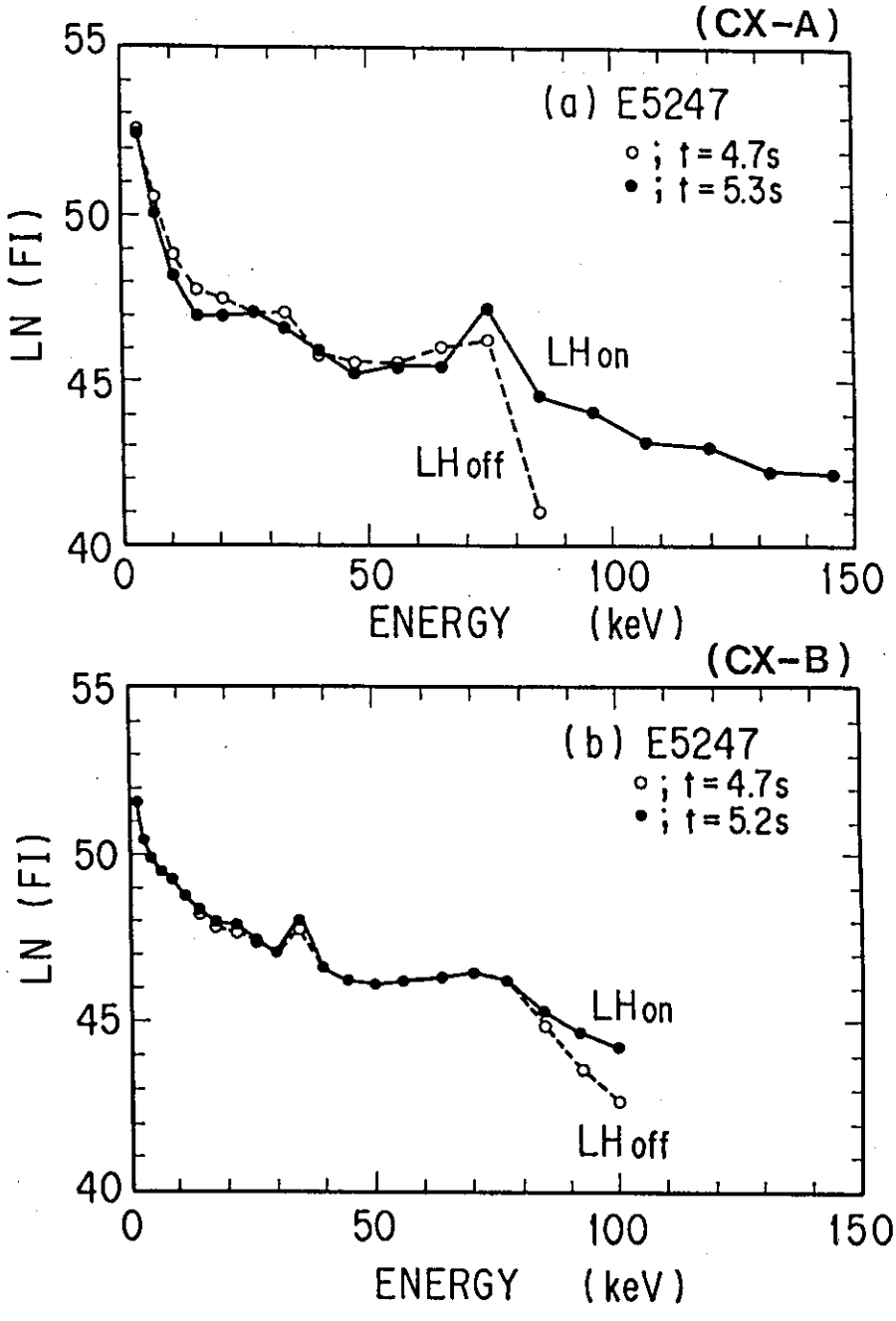

Fig. 10 The neutral particle spectra measured with CX-A (a) and CX-B (b) analyzers for the same shot as shown in Fig. 2. Open and closed circles show neutral fluxes at NB heating phase and NB+LH heating phase, respectively.

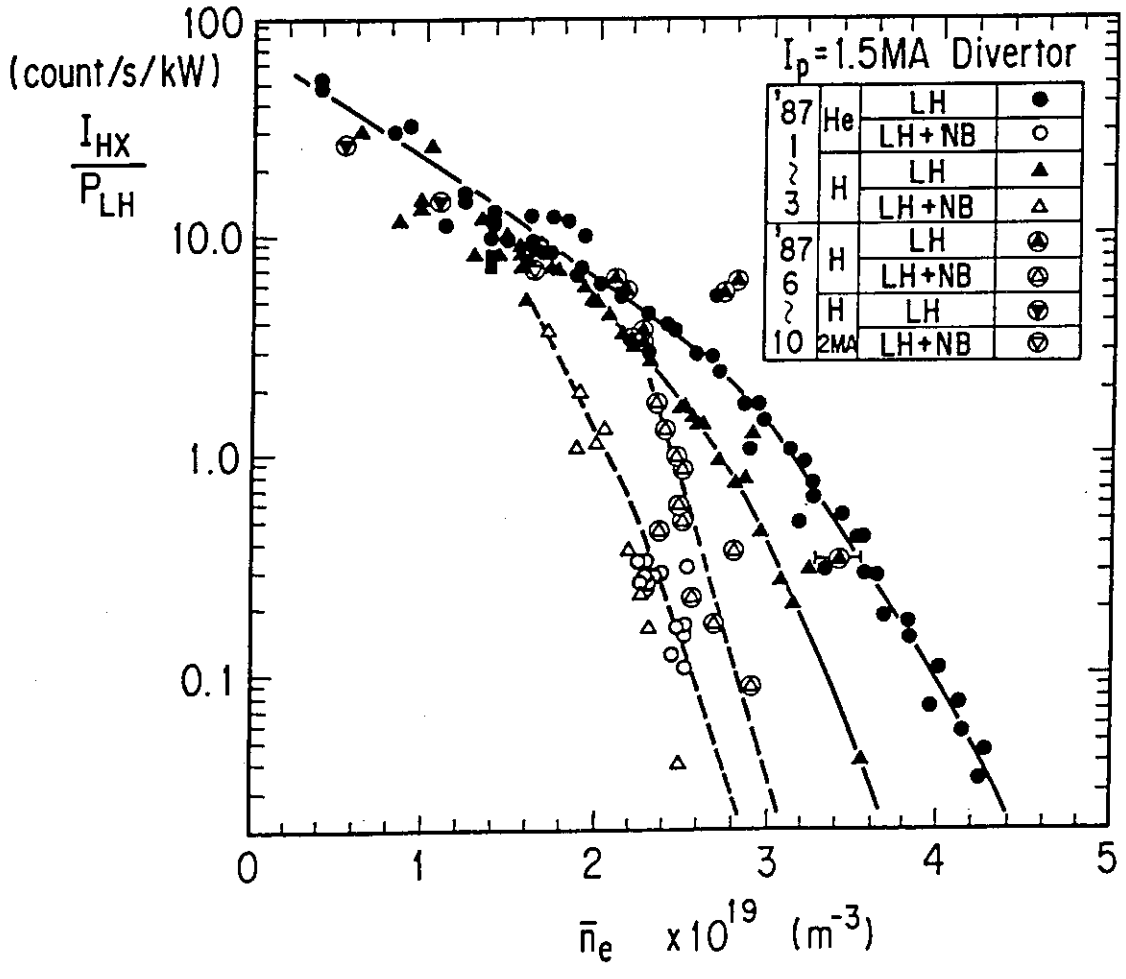

Fig. 11 The plasma hard X-ray intensity (E > 260 keV) normalized by the LH power I_{HX}/P_{LH} against the electron density n_e. Open and closed symbols are for LH alone and LH+NB, respectively.

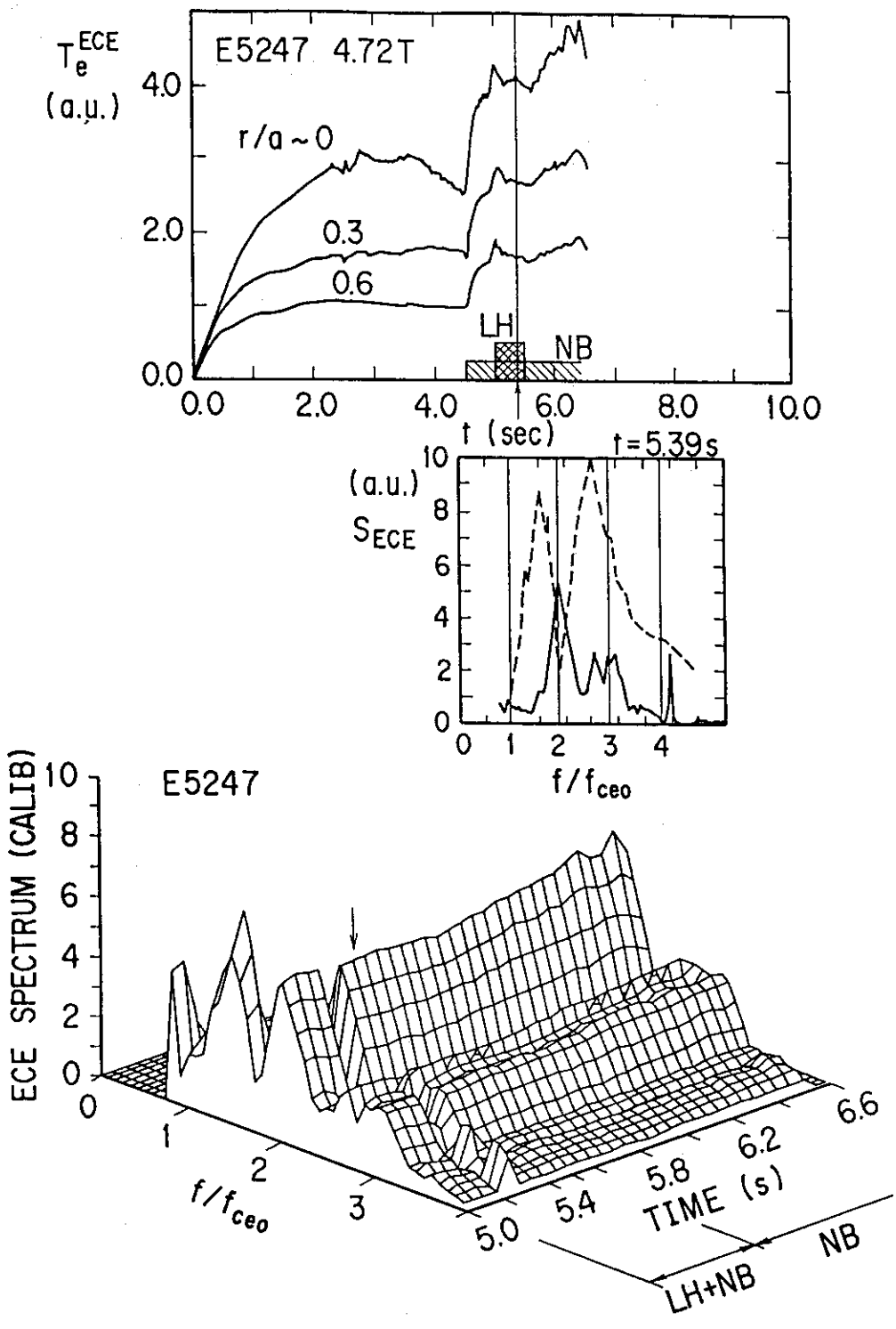

Fig. 12 The ECE signal for the same shot as in Fig. 2. (a); time evolutions of the electron temperature at r/a ∿ 0, 0.3, and 0.6. (b); the frequency spectrum at t ∿ 5.39 s. Typical non-thermal spectrum in the LH heated plasma is shown as a dotted line for reference. (c); time evolution of the ECE spectrum.

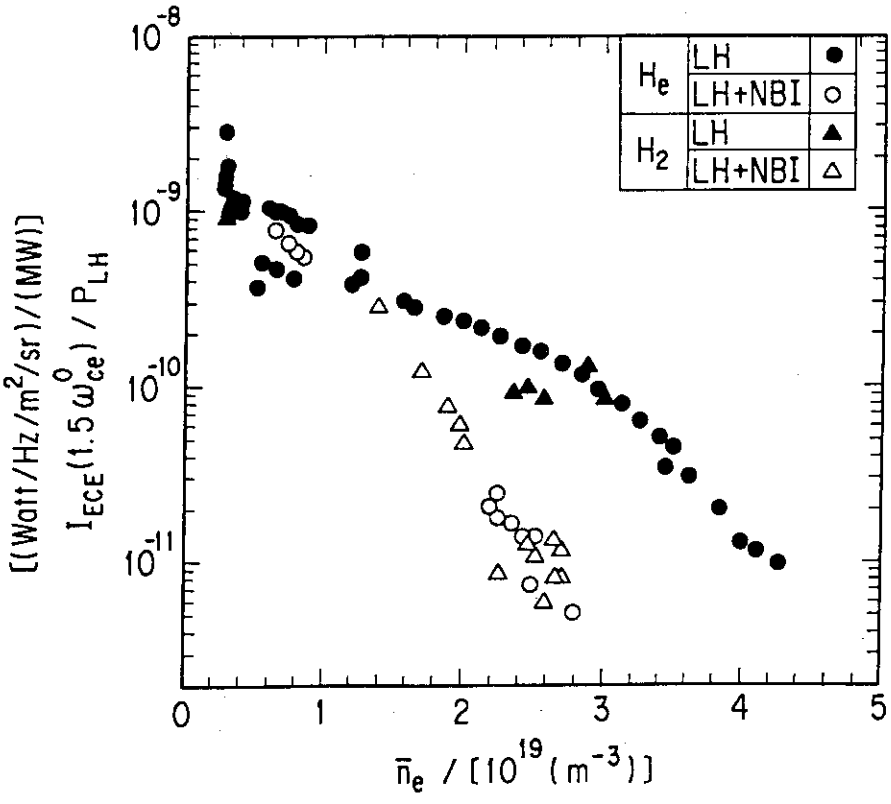

Fig. 13 The density dependence of the 1.5th harmonic ECE signal normalized by the LH power, $I_{ECE}(1.5_{\omega ce})/P_{LH}$.

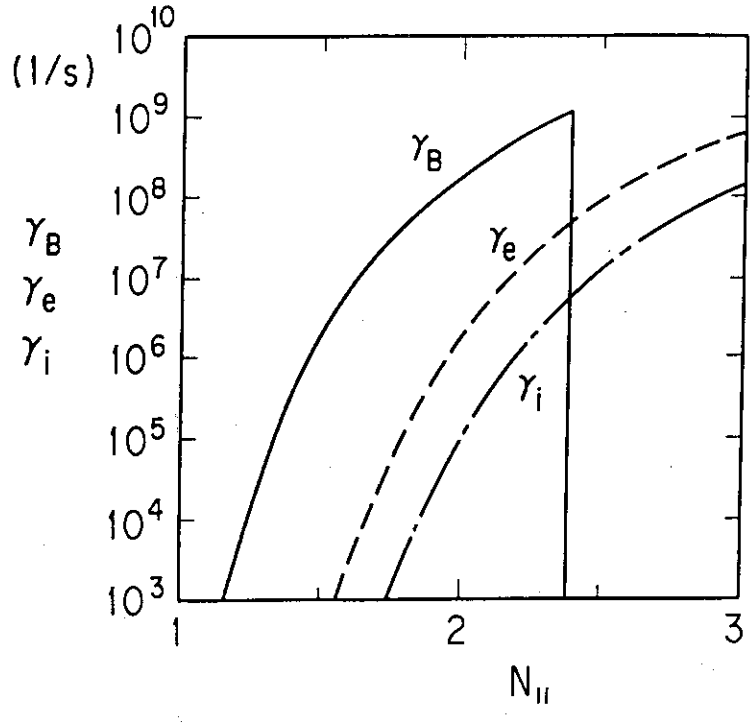

Fig. 14 Wave damping rates due to beam ion (γ_B), bulk electrons (γ_e) and bulk ions (γ_i) as a function of $N_{||}$. These were calculated from following parameters; $n_e = 4 \times 10^{19}$ m^{-3}, $B_T = 4.8$ T, $T_e = 5$ keV, $T_i = 7$ keV, $T_B = 15$ keV, $E_B = 75$ keV, $W_B = 0.4$ MJ and $\omega/2\pi = 2$ GHz.

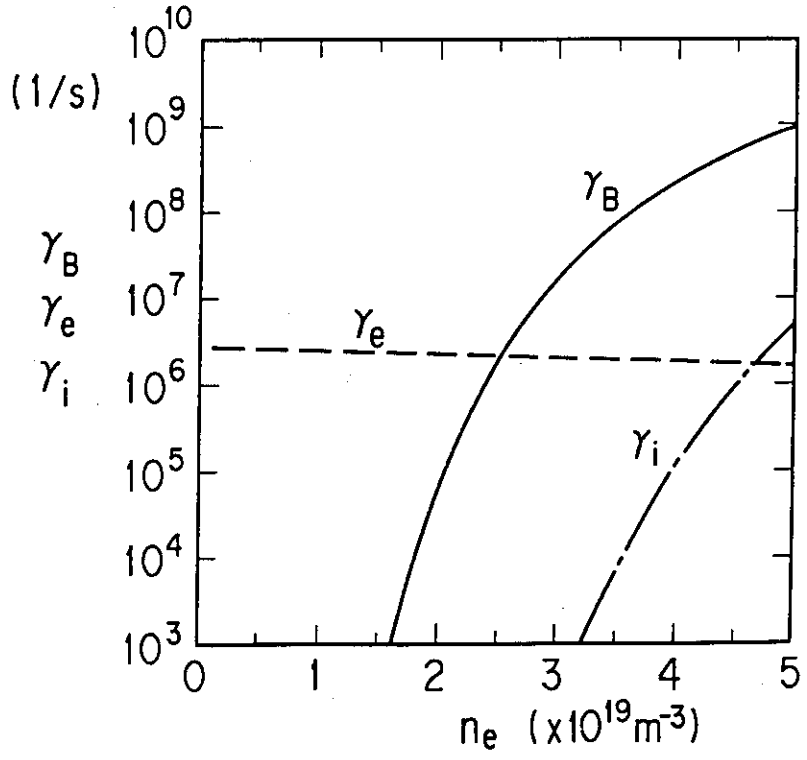

Fig. 15 The density dependence of damping rates. $N_{||}$ = 2.0 and other parameters are the same as in Fig. 13.

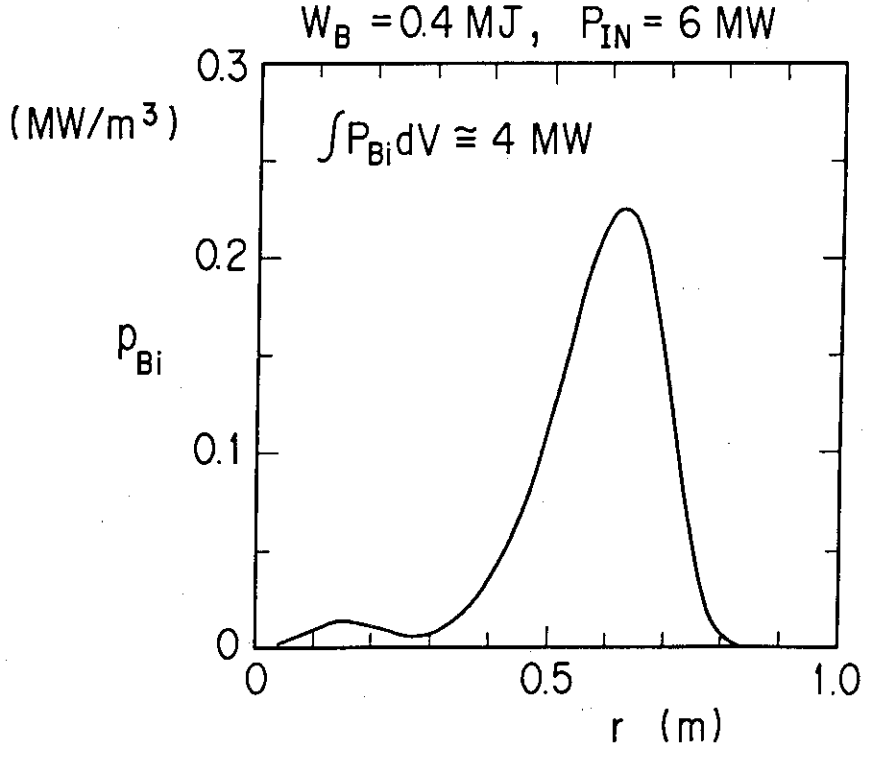

Fig. 17 Power deposition profile to beam ions. Wave spectra for units A and B calculated by Brambilla code with $\Delta\phi$ = 180°. P_{LH} = 6 MW and other parameters are the same as in Fig. 15.

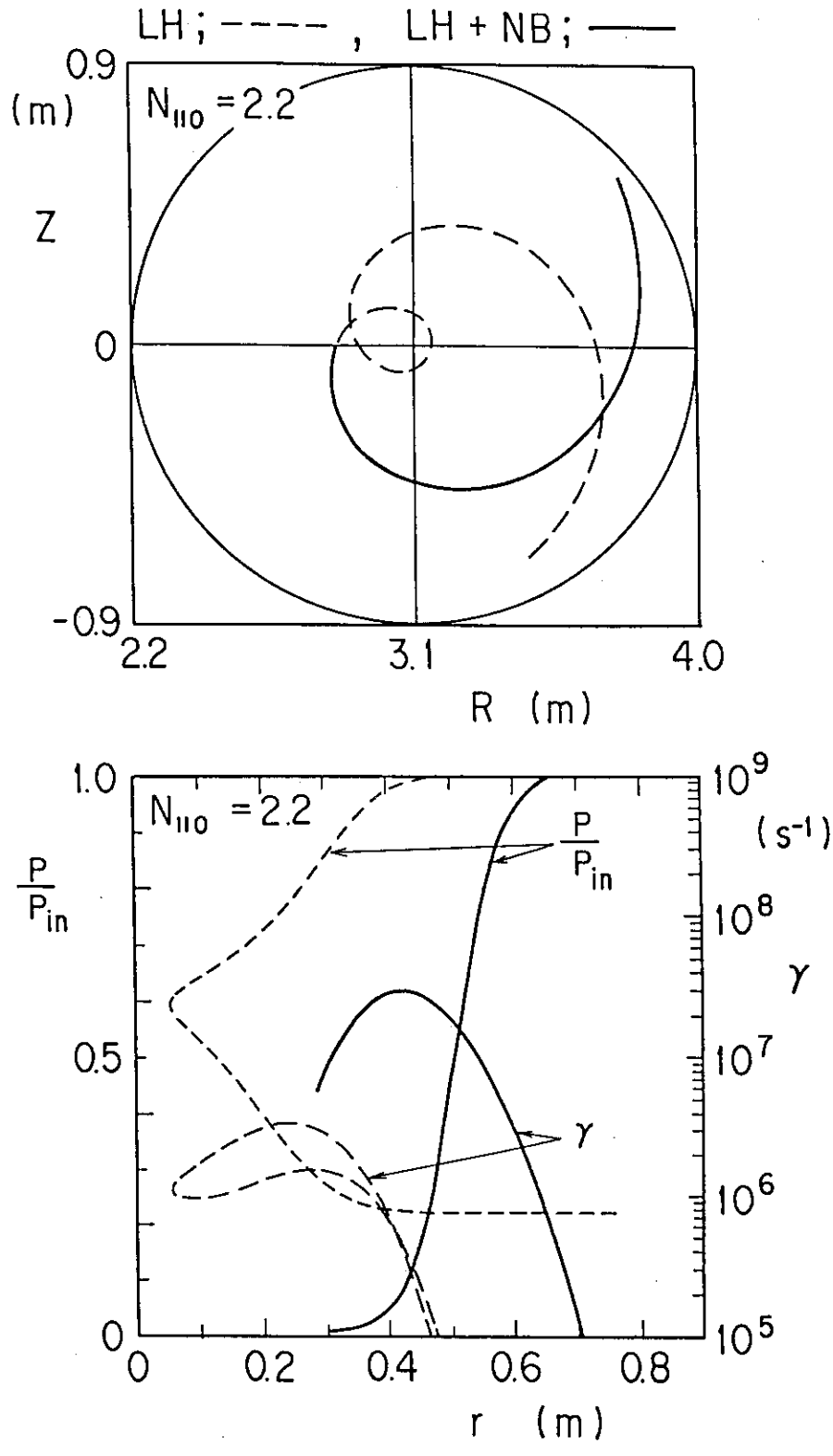

Fig. 16 Ray trajectories for $N_{\|0}$ = 2.2 with and without beam ions (solid line and broken line). We assumed the following parameters; $n_e(0) = 4.2 \times 10^{19}$ m^{-3}, B_T = 4.8 T, $T_e(0)$ = 5 keV, $T_i(0)$ = 7 keV, T_B = 15 keV, E_B = 75 keV, W_B = 0.4 MJ, I_p = 2 MA, $n_e(r) = n_e(0)(1 - r^2/a^2)^{0.32}$, $T_e(r) = T_e(0)(1 - r^2/a^2)^{2.0}$ and $T_i(r) = T_i(0)(1 - r^2/a^2)$.

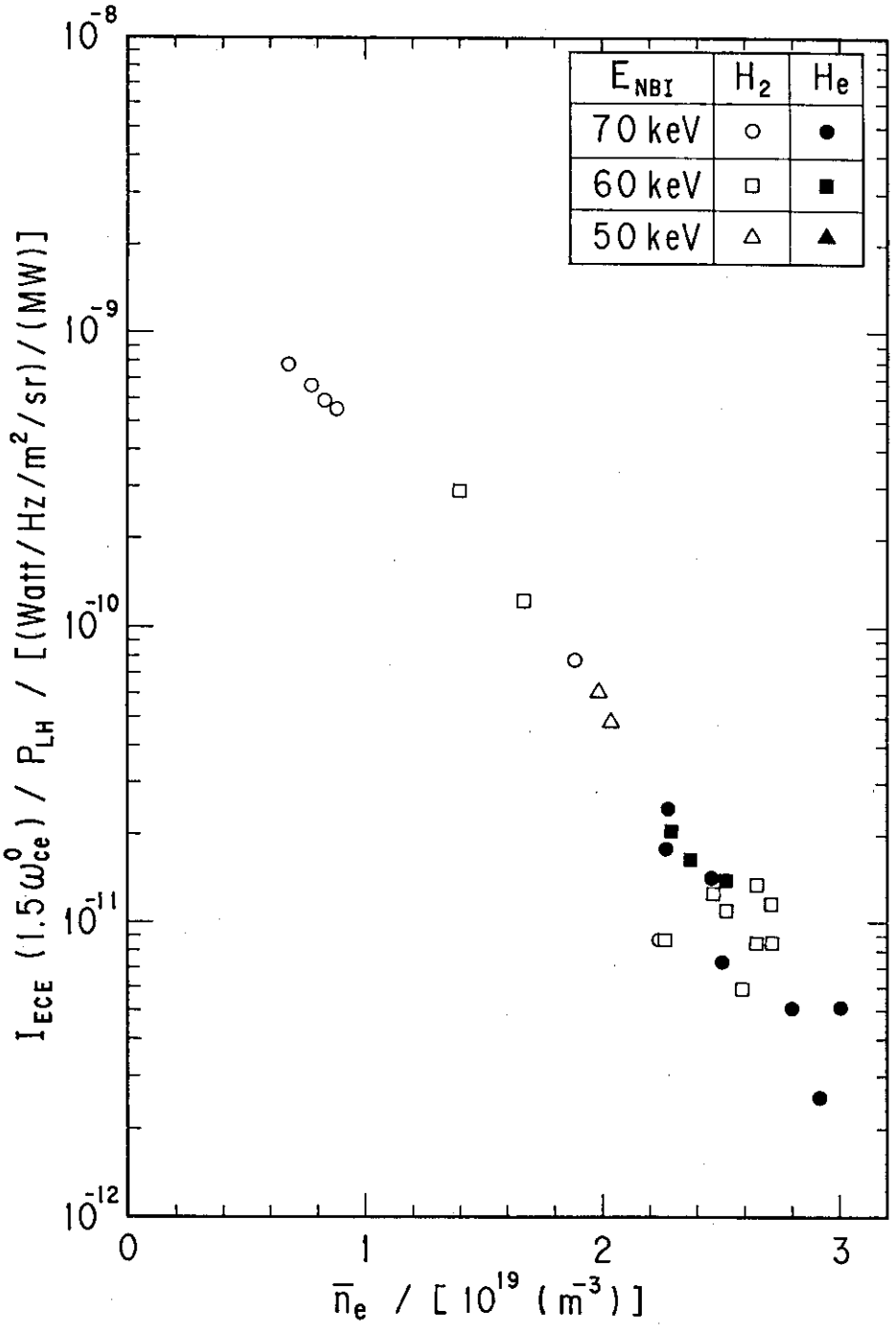

Fig. 18 The 1.5th harmonic ECE signal normalized by the LH power, I_{ECE}/P_{LH} versus the electron density for various beam energies.

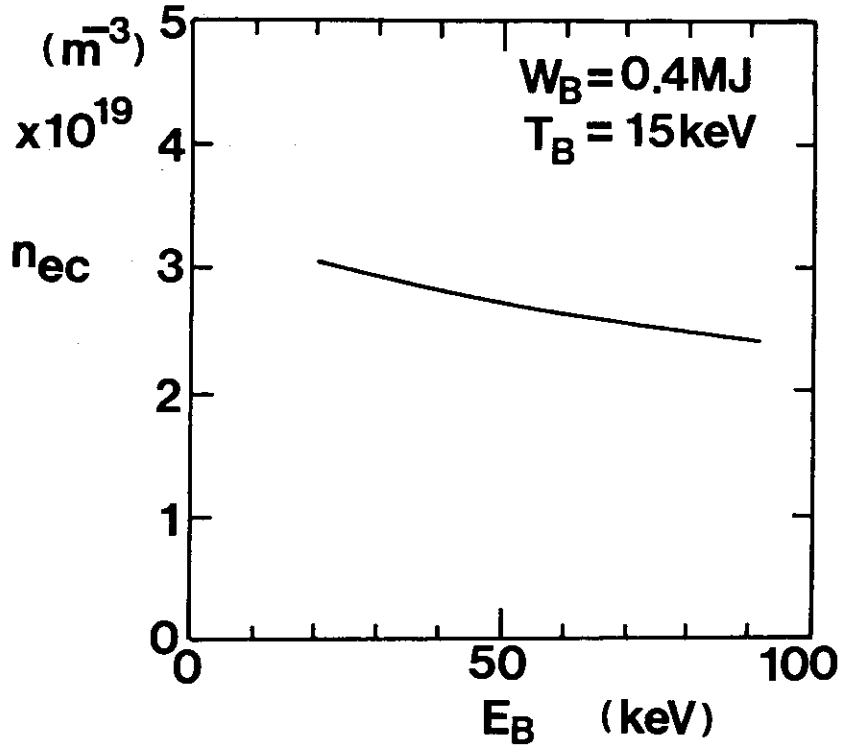

Fig. 19 The critical electron density n_{ec} for $\gamma_e = \gamma_B$ as a function of the beam energy. Other parameters are the same as that in Fig. 15.

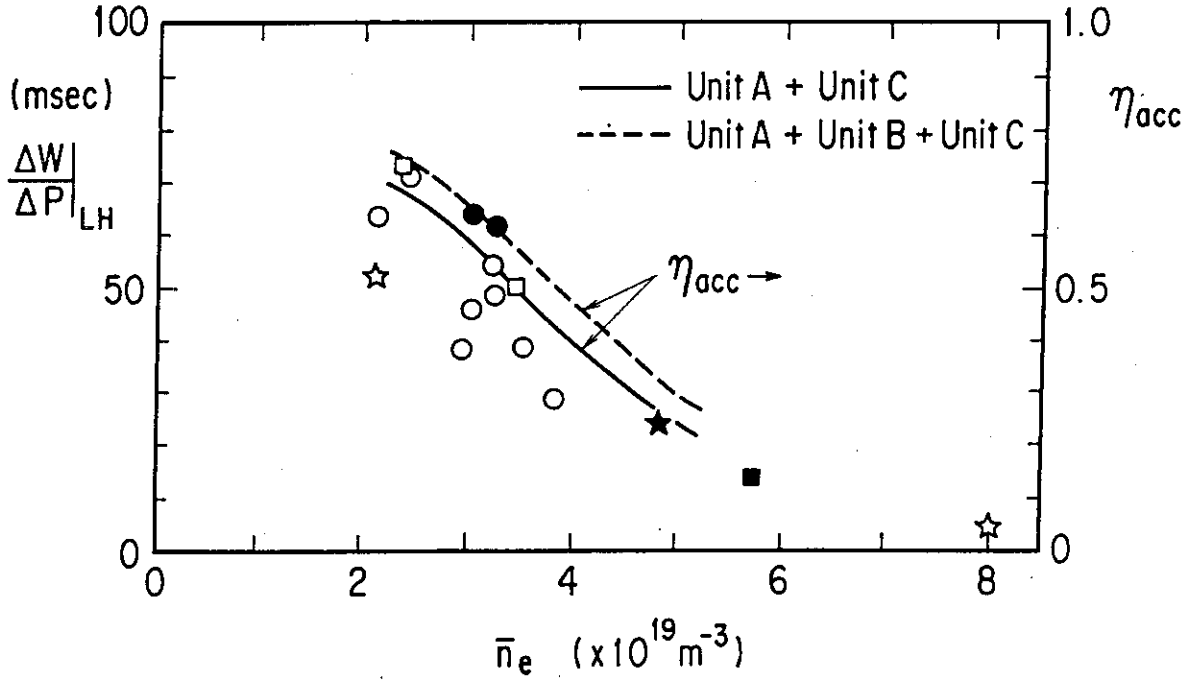

Fig. 20 The density dependence of the fraction of accessible power at half radius estimated using the ray tracing code. Solid and broken lines show the accessible power fraction for waves excited by two units (A and B) and by three units (A, B and C). The heating efficiency shown in Fig. 4 is also plotted. Parameters are the same as in Fig. 15.